Topologically induced semiconductivity in icosahedral Al-Pd-Re and its approximants

M. Krajčí[1,2] and J. Hafner[2]
[1]*Institute of Physics, Slovak Academy of Sciences, Dúbravská cesta 9, SK-84511 Bratislava, Slovak Republic*
[2]*Institut für Materialphysik and Center for Computational Materials Science, Universität Wien, Sensengasse 8/12, A-1090 Wien, Austria*

(Received 22 August 2006; revised manuscript received 23 November 2006; published 30 January 2007)

We demonstrate that the opening of a semiconducting band-gap in the electronic spectrum of the *i*-Al-Pd-Re quasicrystal and its approximants is due to the formation of a topological band-gap, in analogy to the band-gap found in the FeSi (*B*20) structure. In both systems we have identified a network of linear chains of alternating Si(Al) and transition-metal (TM) atoms extending along twofold symmetry directions. In *i*-Al-Pd-Re the chains of alternating Al and TM atoms extend from a center of the pseudo-Mackay (*M*) cluster over the surface of the Bergman cluster to the center of another neighboring *M* cluster. Substitutional Al/Pd defects and a fragmentation of the chains by phason defects lead to the formation of localized states in the band-gap. The band-gap of the real *i*-Al-Pd-Re quasicrystal is filled by localized states. The *i*-Al-Pd-Re quasicrystal thus behaves as a disordered semiconductor.

DOI: 10.1103/PhysRevB.75.024116 PACS number(s): 61.44.Br, 71.20.−b, 71.23.Ft, 71.55.−i

I. INTRODUCTION

To elucidate the conditions under which materials show metallic or insulating behavior is one of the fundamental issues of solid-state science. According to Bloch-Wilson theory[1] a system is metallic if at least one of its energy bands is only partially occupied by electrons and an insulator or a semiconductor if all bands are either completely full or empty. However, it is well known that certain classes of materials, which should be metals according to Bloch-Wilson theory, are insulators instead. A first example is compounds of transition- and rare-earth metals where the strong local Coulomb interaction between electrons occupying the narrow *d* or *f* band promotes a large exchange splitting and the formation of a band-gap at the Fermi level, transforming a metal to a Mott insulator.[2] A second mechanism transforming metallic into insulating behavior consists in strong spin fluctuations leading to the formation of a Kondo insulator.[3] Such systems are considered as being dominated by strong many-body correlations.

A mechanism not related to many-body effects, but still inducing the opening of a band-gap in an otherwise metallic system, is a Peierls distortion. The simplest examples for materials with a Peierls instability[4] are the elements of groups V and VI of the periodic table. For these elements, bonding is mediated by the *p* electrons only and the angular character of the *p* orbitals naturally supports the formation of a simple cubic crystal lattice. However, for these materials the *p*-band complex is just half (group V) or two-thirds (group VI) filled, and this leads to a dimerization or a trimerization of the lattice, accompanied by the formation of a narrow gap at the Fermi level.[5] Peierls instabilities exist also in a number of binary compounds,[6] and it is a characteristic feature of the Peierls mechanism that a change in the electron-per-atom ratio also induces a change in the periodicity of the lattice distortion, the Peierls gap opening always at the Fermi level. This is different from the behavior of certain intermetallic compounds, mainly transition-metal (TM) aluminides and silicides (e.g., $RuAl_2$, $RuGa_2$, and $CrSi_2$ crystallizing in the *C*54 structure[7] and FeSi adopting the *B*20 structure) also showing a narrow gap at the Fermi level. We have recently been able to show[8] that for these materials gap formation arises from the bonding-antibonding splitting of the Al-TM *s*,*p*-*d* hybrid orbitals forming strong, partially covalent Al-TM bonds. We have been able to show that similar gaps exist in a wide range of binary and ternary[9] TM-dialuminides with the *C*40 ($CrSi_2$), *C*54 ($TiSi_2$), and $C11_b$ ($MoSi_2$) structures. The location of the gap always obeys a 14-electron (per formula unit) rule, but a gap exists also in electron-deficient (e.g., $MnAl_2$) or electron-enriched (e.g., $CoAl_2$) compounds, although in these cases the Fermi level is located below or above the gap. This creates a distinctive difference with respect to Peierls-instable system were the gap is pinned at the Fermi level. Gap formation in the TM-aluminides is dependent on the topology of the crystalline lattice, and we refer to the energy gap in these systems as the *topological energy gap*. Very recently Frederickson *et al.*[10,11] have pointed out that the arguments put forward for the TM-dialuminides also apply to a wide class of compounds between transition metals and main-group elements, the so-called Nowotny chimney ladder phases.[12]

The discovery of quasicrystals has added a new facet to the problem of metal-insulator transitions (MITs). Many quasicrystals show a high residual resistivity, a negative temperature coefficient of the electrical resistivity, and a magnetoresistance similar to that of doped semiconductors.[32] One of the most extensively studied systems is icosahedral (*i*) Al-Pd-Re quasicrystals. It has been demonstrated that samples of *i*-Al-Pd-Re with high crystalline perfection are definitely on the insulating side of the MIT.[33,34] Using *ab initio* electronic structure calculations we have been able to show that a class of icosahedral aluminum–transition-metal quasicrystals shows semiconducting behavior due to the formation of a narrow gap at the Fermi level. However, the decisive question regarding the physical mechanism of the MIT in these quasicrystal has remained unanswered so far. The aim of the present work is to demonstrate that the band-gap in the icosahedral quasicrystals is topologically induced,

in analogy with the crystalline Al-TM compounds.

A narrow indirect semiconductor gap of ~0.13 eV has also been found, both experimentally[13–17] and theoretically[18–24] in cubic FeSi. Because of the highly unusual temperature dependence of the magnetic susceptibility and of the electronic transport properties, FeSi has initially been considered as a correlated electron insulator, but it has been demonstrated that the existence of a narrow band-gap is predicted quite accurately by density functional theory as a consequence of its crystalline structure with a nonsymmorphic $P2_13$ space group and that the temperature dependence of the electronic and magnetic properties is a consequence of thermal disorder and Fermi-Dirac smearing. The $B20$ structure of FeSi may be considered as being derived from the $B1$ (NaCl) structure by a distortion involving a displacement of Fe or Si atoms along [111] directions. These distortions are large (leading to an energy gain of about 1.6 eV/formula unit) and reduce the space-group symmetry from $F3m3(O_h^5)$ to $P2_13(T^4)$. The nonsymmorphic space group leads to an unusual band-structure in the vicinity of the Fermi level, with rather peculiar fourfold-degenerate bands at the R point, a "sticking" of pairs of bands over the entire Brillouin-zone surface, and the opening of a narrow gap at the Fermi level, arising from the bonding-antibonding splitting in the middle of the Fe-d–Si–p band complex. The fact that the gap opening in FeSi is a consequence of the topology of the crystalline lattice and not driven by the Fermi-surface effects dominant in systems undergoing a Peierls distortion is also supported by the fact that the $B20$ structure occurs[25] in the entire series of compounds CrSi, MnSi, FeSi, and CoSi where the average number of filled bands increases from 20 to 26. For MnSi band structure calculations[23,26] predict a narrow energy gap of ~0.12 eV at the band filling appropriate to FeSi—i.e., above the Fermi level. Another view of the $B20$ structure in terms of an "ideal $B20$" structure has been proposed by Vočadlo *et al.*[27] In the $B20$ structure both Fe and Si occupy $(4a)$-type sites in the simple cubic unit cell, with position coordinates[28] of $u(\mathrm{Fe})=0.1358$ and $u(\mathrm{Si})=0.844$. Moving the atoms to $u(\mathrm{Fe})=0.25$ and $u(\mathrm{Si})=1-u(\mathrm{Fe})=0.75$ induces a transformation to the $B1$ structure, while for $u(\mathrm{Fe})=1/(4\tau)=0.1545$ and $u(\mathrm{Si})=1-1(4\tau)=0.8455$ [where $\tau=(1+\sqrt{5})/2$ is the golden mean] each atom has exactly 7 nearest neighbors of the opposite kind at a distance of $a\sqrt{3}/(2\tau)$. The 7 nearest neighbors occupy 7 of the 20 vertices of a pentagonal dodecahedron centered at the atom. The sevenfold coordination and the arrangement of the coordinating atoms have led Dmitrienko[29] to interpret the $B20$ structure as a low-order crystalline approximant to an icosahedral quasicrystal—indeed we will demonstrate that this structural relation is the key to the understanding of the unusual electronic properties of these materials.

To demonstrate the relation of the $B20$ structure to icosahedral quasicrystals more explicitly, let us consider the nearest-neighbor bonds between Fe and Si atoms as edges of a tiling. Then the elementary cell of the $B20$ structure can be interpreted as a tiling of four prolate and four oblate rhombohedra. However, these rhombohedra are not identical with the golden rhombohedra that constitute the three-dimensional Penrose tiling. The bonds in the ideal $B20$ structure with the parameter $u(\mathrm{Fe})=1/(4\tau)$ are oriented along the threefold-symmetry axes (yellow sticks in the well-known Zometool construction kit[30]). We note that if $u=1/(4\tau^2)=0.095$, one gets a "golden $B20$" tiling (built from red sticks[30]) that consists of golden prolate and oblate rhombohedra. The bonds are oriented along the fivefold-symmetry axes. Such a structure can be denoted as a 1/0 approximant in the hierarchy of periodic Penrose tilings. However, the vertices of such a structure cannot be occupied by individual atoms because of the short interatomic distances in the oblate rhombohedra. Nevertheless, if the size of the tiling is properly rescaled and the vertices are occupied by clusters with icosahedral symmetry (Mackay and Bergman), one immediately obtains a model of a 1/1 approximant to the F-type icosahedral quasicrystal. Considering the scaling of the size of the elementary cells in the hierarchy of the periodic Penrose tilings one can conclude that the ideal $B20$ structure is a 0/1 approximant in this hierarchy. The relation of the ideal $B20$ to icosahedral quasicrystals can also be seen through the concept of the canonical cells introduced by Henley.[31] The ideal $B20$ structure is a canonical cell tiling consisting of 24 A cells, 8 B cells, and 8 C cells. If the threefold bonds in the $B20$ structure are replaced by the golden prolate rhombohedra and the nearest-neighbor bonds along the twofold axes (blue sticks[30]) replaced by the golden rhombic dodecahedra, one gets a 2/1 approximant to the F-type icosahedral quasicrystal. The size of the Penrose tiles in this quasicrystalline approximant is related to the size of the canonical cells by the factor τ^3. One can thus again recognize the ideal $B20$ structure as a 0/1 approximant in the hierarchy of approximants to the F-type icosahedral quasicrystal.

Indeed the key to an understanding of the semiconducting properties of i-Al Pd Re can be found in the structural relationship between the icosahedral quasicrystal and the $B20$ structure, which is a low-order 0/1 approximant to the infinitely extended quasicrystal. We demonstrate that the network of alternating strong and weak TM-Si(Al) bonds characteristic of the $B20$ phases exists throughout the hierarchy of the quasicrystalline approximants and that it is this characteristic topology that determines the semiconducting behavior of the quasicrystals.

Our paper is organized as follows: In Sec. II we briefly recapitulate our knowledge of the electronic properties of i-Al-Pd-Re; our structural model for the icosahedral phase is described in Sec. III. The computational setup is defined in Sec. IV. In Sec. V we discuss the mechanism leading to the formation of a band-gap, concentrating on the topological similarities between the $B20$ structure and the quasicrystal. Localized gap states created by the introduction of lattice defects are discussed in Sec. VI, and we summarize in Sec. VII.

II. ELECTRONIC PROPERTIES OF i-Al-Pd-Re: THE STATE OF THE ART

A. Electronic structure and transport: Experiment

The puzzling insulatorlike properties of icosahedral Al-Pd-Re quasicrystals have excited physicists' interest already

for more than a decade. The low-temperature electrical conductivities of some *i*-Al-Pd-Re samples are in the same range [$\rho(4.2\ \mathrm{K}) \approx 1\ \Omega\,\mathrm{cm}$] as for doped semiconductors. Icosahedral Al-Pd-Re samples can be prepared with various low-temperature resistivities ρ and resistance ratios $R = \rho(4.2\ \mathrm{K})/\rho(295\ \mathrm{K})$. Although there is no deeper theoretical background for understanding the role of the R parameter in determining the transport mechanism, this parameter is used as a measure of the quality of the samples. It was shown[33,34] that samples with low R value exhibit metallic conductivity, while samples with a high R value are insulating. So far there is no common agreement on the critical value of the R parameter determining the metal-insulator transition.

Many studies have been devoted to the temperature dependence of the transport properties at very low temperatures. Delahaye *et al.*[35] showed that the conductivity $\sigma(T)$ follows Mott's variable-range hopping (VRH) conduction law[36] $\sigma(T) = \sigma \exp[-(T_0/T)^p]$, with $p = 1/4$, in the temperature range 20–600 mK. The same temperature dependence was also deduced from anomalous Hall effect measurements.[37] Srinivas *et al.*[38] studied magnetoresistance at 1.5–8 K and in magnetic fields up to 12 T. The observed temperature and field dependences in samples with high R parameter follow a VRH law of the Efros-Shklovskii (ES-VRH) type,[39] differing from Mott's law by the exponent $p = 1/2$. From the analysis of magnetoresistance data Su *et al.*[40,41] report a crossover from Mott VRH conduction to ES-VRH conduction at liquid helium temperatures. A complex low-temperature scaling of resistivity and magnetoresistance has been observed also by Rosenbaum *et al.*[42,43] The accumulated experimental data indicate that the MIT in high-resistive *i*-Al-Pd-Re samples is disorder driven. Karkin *et al.*[44] studied an insulator-to-metal transition in *i*-Al-Pd-Re induced by neutron irradiation. Irradiation over a wide range of doses preserves the icosahedral long-range order, but an increasing amount of defects monitored by a decreasing diffraction peak intensity leads to a decrease of the R parameter. A similar result was also obtained by Préjean *et al.*[45] who observed a linear increase of the conductivity with the concentration of the local defects in *i*-Al-Pd-Mn quasicrystals.

An understanding of the relation between quasicrystalline perfection and insulating properties of some *i*-Al-Pd-Re samples seems to be essential for understanding the origin of their semiconducting properties. It is obvious that the MIT observed in *i*-Al-Pd-Re has nothing in common with the MIT due to the Anderson localization of electronic eigenstates known to occur in disordered systems. While in these systems increasing disorder can lead to an insulating state, in *i*-Al-Pd-Re quasicrystals increasing disorder leads to an increase of conductivity. One could thus assume that a "perfect" *i*-Al-Pd-Re quasicrystal without any disorder behaves like an ordinary semiconductor. Berger *et al.*[46] report a striking similarity of the tunneling conductance of *i*-Al-Pd-Re with ordinary disordered semiconductors. Similarities are observed between the direct and tunneling conductivities of disordered systems on both sides of the MIT.[46] In *i*-Al-Pd-Re quasicrystals as in ordinary semiconductors the conductivity decreases with decreasing temperature. An extrapolation of the temperature dependence of the conductivity $\sigma(T)$ below 1 K down to 0 K shows a saturation of the conductivity[34] at a nonzero value $\sigma(0\ \mathrm{K})$. This estimated $\sigma(0\ \mathrm{K})$ value was found to decrease strongly (over four orders of magnitude[47]) with increasing resistance ratio R. Although highly resistive *i*-Al-Pd-Re seems to have much in common with an ordinary semiconductor, no experiment so far indicates the opening of a real gap in the electronic spectrum of *i*-Al-Pd-Re as in ordinary semiconductors. On the other hand, a significantly reduced electronic density of states (DOS) was reported by specific-heat measurements[48,49] and by electron spectroscopy.[50,51] Tunneling spectroscopy[52,53] and nuclear magnetic resonance[54] measurements also indicate a rapidly varying DOS around the Fermi level.

Much effort has been spent with the aim to understand the mechanism of the anomalous transport properties of *i*-Al-Pd-Re quasicrystals. Since the discovery of quasicrystals, many authors expressed a suspicion that the anomalously high resistivities of many quasicrystals might be related to quasiperiodicity itself.[55] The same was assumed also for the high-resistive *i*-Al-Pd-Re quasicrystal. Although this question still remains open,[56,57] there now exists growing evidence that this is not the case. It was shown[58,59] that an infinite quasiperiodic system has low, but still metallic conductivity. The fact that periodic approximants to quasicrystals have similar transport properties as infinite quasicrystals indicates that it is the structural complexity rather than quasiperiodicity that contributes to the enhanced resistivity of order $m\Omega$ cm observed in many quasicrystals; see, e.g., the review article by Rapp.[32]

We assume that most of the experimentally reported facts on anomalous transport properties presented above are consistent with a picture of *i*-Al-Pd-Re as a disordered semiconductor. In the present work we attempt to elaborate the physical background for such a picture. Particularly, we shall try to shed light on the mechanism of the semiconducting band-gap formation in this metallic alloy and also explain the origin of localized states in the semiconducting band-gap in any real (i.e., partially disordered) sample of *i*-Al-Pd-Re.

B. Electronic structure: Calculations

In a previous paper[60] we have already demonstrated that a special class of aluminum–transition-metal quasicrystals exhibits semiconducting properties. All belong to the face-centered-icosahedral (F-type) class, which is also the case for icosahedral Al-Pd-Re. a special ordering between aluminum and transition-metal atoms in the quasicrystalline structure, expressed by the shell structure of the atomic acceptance domains in six-dimensinal (6D) hyperspace leads to the surprising disappearance of its metallic character, caused by the formation of a narrow band-gap in their electronic spectrum. As it is generally expected that alloys composed of metallic elements are metallic too, the existence of such a band-gap is very peculiar. The width of the gap can be of order of some tenths of eV. The exact physical mechanism leading to band-gap formation has not yet been explained. Semiconducting behavior has been observed in low-order approximants to F-type quasicrystal. We were able to demonstrate the existence of truly semiconducting 1/1 approximants, and semiconducting behavior has also been

established for a 2/1 approximant with 544 atoms per unit cell.

Structural relaxation has been found to be very important for band-gap formation. A structural model with idealized coordinates as obtained by projection from 6D space exhibits either no real gap or only a very narrow band-gap. During structural relaxation the forces acting on the atoms move them from the idealized to their force-free equilibrium positions. The quasicrystalline structure becomes displacively modulated, and interatomic distances between Al and TM atoms are contracted. A network of chemical bonds with enhanced covalency is formed. The enhanced covalency of interatomic bonding has been confirmed also experimentally.[61,62] Although the shifts of the atoms from their original positions are rather small (of order of some tenths of Å), the influence of the relaxation on the electronic structure is important.

Semiconducting 1/1 *approximants*

The existence of a band-gap has been found to be very sensitive to a particular ordering between aluminum and transition-metal atoms. In the Katz-Gratias-Boudard (KGB) model this ordering is defined in 6D hyperspace by the shell structure of the occupation domains in perpendicular space. Any deviation from this ordering leads to the appearance of localized states in the band-gap. At a certain band filling corresponding to a well-defined stoichiometry (Al/TM ratio) the Fermi level falls into the gap. The critical band filling differs slightly for each approximant. On the other hand, a band-gap exists for different combinations of transition metals. We demonstrated the existence of a gap for various concentrations of TM elements from group 4 to group 11. It is remarkable that on the one hand the existence of a gap depends sensitively on the aluminum–transition-metal ordering (a single substitution defect leads to the formation of states in the gap and a higher defect concentration can even close the gap), whereas on the other hand the interchange of different TM atoms has only a modest effect on the gap.

The position of the band-gap with respect to the Fermi level depends on the band filling. In the KGB model the composition ratio Al/TM is fixed by the shell structure of the occupation domains. The band filling can be varied by the choice of the valency and the concentration of TM atoms in the alloy. For a binary Al-TM system with TM atoms of group 9 the gap is above the Fermi level; for group 10 the gap is already below the Fermi level. In a ternary AL-TM_1-TM_2 system with two different TM elements a proper combination of the TM elements from two different groups can shift the position of the Fermi level exactly to the gap. The band-gap becomes wider if TM atoms are 5*d* metals; for 4*d* and 3*d* metals the width of the gap is generally smaller. This dependence is apparently related to the spatial extension of *d* states which is largest for 5*d* metals. In the case of a 1/1 approximant with 128 atoms per unit cell the critical band filling is 648 electrons. The band-filling condition of 648 electrons/cell is met for three stoichiometries: $Al_{88}M(10)_{24}M(9)_{16}$, $Al_{88}M(10)_{36}M(6)_4$, and $Al_{88}M(11)_{12}M(9)_{28}$, where $M(i)$ is a transition-metal atom with i number of valence electrons. Considering all combinations of TMs from the 3*d* to 5*d* rows, these rules determine the composition of many possibly semiconducting 1/1 approximants. In Ref. 60 we have calculated the electronic structure and demonstrated semiconducting behavior for several ternary alloys. As Re has seven valence electrons, an approximant to *i*-Al-Pd-Re does not belong to any of these three stoichiometry classes. For a 1/1 Al-Pd-Re approximant the band-gap falls either just above the Fermi level or is closely below the Fermi level. However, the stoichiometry criterion for critical band filling is easier to satisfy with an increasing size of the approximant.

In this paper the semiconducting behavior of this special class of *F*-type icosahedral quasicrystals is further explored with particular attention to *i*-Al-Pd-Re approximants. In Sec. V we investigate the mechanism for band-gap formation in detail. We shall show that the mechanism of band-gap formation in the Al-Pd-Re quasicrystal is essentially the same as in the *B*20 (FeSi) structure (which may be considered as a 0/1 approximant to the quasicrystal) and related to the topology of the quasicrystalline lattice. In Sec. VI we discuss the formation of localized states in the electronic spectrum of Al-Pd-Re approximants. In Sec. VII we summarize the results and discuss possible consequences of character of the electronic spectrum of Al-Pd-Re on its transport properties.

III. STRUCTURAL MODEL

The icosahedral Al-Pd-Re quasicrystal belongs to the *F*-type quasicrystals. Diffraction data and the identical stoichiometry of Al-Pd-Re and Al-Pd-Mn quasicrystals indicate that Al-Pd-Re and Al-Pd-Mn are essentially isostructural. A six-dimensional model of *F*-type quasicrystals has been proposed by several authors; it is usually referred as the Katz-Gratias[63,64] (KG) model. The KG model is defined by three occupation domains with the form of triacontahedra decorating a 6D lattice. On the basis of the KG model Boudard and co-workers[65,66] proposed a structural model for the icosahedral Al-Pd-Mn quasicrystal. In their approach the chemical identity of individual atoms is determined by a simple spherical shell structure of the occupation domains. We combined these ideas and proposed a 6D model of Al-Pd-Mn where the internal shells of the occupation domains have shapes of concentric triacontahedra.[60] The model is labeled as the Katz-Gratias-Boudard model. The KGB model is described in detail in our previous papers.[60,67] As in the KG model, our model consists of three occupation domains. They decorate the even (n_0) and odd (n_1) vertices and the odd body-center positions (bc_1) of a 6D hypercubic lattice. The two occupation domains located at n_1 and bc_1 have the shape of a triacontahedron, which on n_0 is a truncated triacontahedron. The n_0 and n_1 domains have an internal shell structure. The ratio of the diameters of the internal shells is expressed in terms of simple multiples of powers of the golden mean τ. Each part of the domain corresponds to a specific chemical type. Aluminum atoms occupy the outer parts of the n_0 and n_1 domains; TM atoms occupy the inner parts of the domains. The bc_1 domain is occupied by TM atoms only. This simple rule defines the Al-TM ordering that has been found to be essential for the semiconducting behavior.

The KGB model proved to be quite successful as a structural model of Al-Pd-Mn icosahedral quasicrystals.[65,67] The model agrees well with the diffraction data, density, and stoichiometry.[63,65,68,69] The stoichiometry of the Al-Pd-Mn quasicrystal predicted by the KGB model, $Al_{0.7073}Pd_{0.2063}Mn_{0.0864}$, is in very good agreement with the experimentally determined composition of $Al_{0.711}Pd_{0.202}Mn_{0.087}$ (Ref. 70) or $Al_{0.705}Pd_{0.21}Mn_{0.085}$ (Ref. 35). The KGB model also provides very good agreement of the calculated photoemission spectra with experiment.[71] Recently the KGB model has been used to construct a model of the fivefold surface of *i*-Al-Pd-Mn.[72] The model predicts the existence of surface vacancies, and a comparison of the calculated scanning tunneling microscopy (STM) images with the experimental ones revealed that some characteristic features of the STM images known as the "dark pentagonal stars" can be identified with these surface vacancies.[73] For the purpose of electronic structure calculations this model is the most suitable. The reason is not only its satisfactory description of the chemical ordering, but the simplicity of this model in 6D space which allows us to impose a linear phason strain and thus to construct well-defined finite approximants.

Other, more sophisticated structural models of *i*-Al-Pd-Mn also exist. Papadopolos co-workers proposed a tiling model of *i*-Al-Pd-Mn,[74,75] called the $\mathcal{M}$ model. They decorated a 3D Penrose tiling in accordance with the *F* character of the 6D lattice. In its 6D representation the $\mathcal{M}$ model also has three atomic surfaces like the KG model, but their shapes are somewhat more complex. Yamamoto *et al.*[76,77] proposed an even more sophisticated model for *i*-Al-Pd-Mn with complex occupation domains. Unfortunately, in these models the Al-TM ordering that is so crucial for band-gap formation is not well defined. Parts of the occupation domains have mixed Al/TM occupancies. Although such models are eventually more realistic than our KGB model, they are not appropriate for *ab initio* electronic structure and total energy calculations. A remarkable model of *i*-Al-Pd-Mn has been proposed also by Quandt and Elser.[78] It is a model based on *ab initio* simulations. The model has been further improved by Zijlstra. *et al.*[79] Although the size of the model is 65 atoms/cell only, the model provides a resonable stoichiometry and a good agreement of the calculated photoemission spectrum with an experiment.[79]

IV. COMPUTATIONAL PROCEDURE

We have used advanced local-density-functional techniques to perform a series of *ab initio* electronic structure calculations for a sequence of quasicrystalline approximants. The electronic structure for different chemical compositions has been calculated using the Vienna *ab initio* simulation package VASP.[80,81] VASP performs a variational solution of the Kohn-Sham equations in a plane-wave basis, using projector-augmented-wave potentials for describing the electron-ion interaction. Electronic exchange and correlation are treated in the generalized gradient approximation.[82] The calculation of the Hellmann-Feynman forces acting on the atoms allows one to perform a full optimization of the atomic positions in the unit cell and of the lattice parameters. The relaxation reflects the formation of a network of chemical bonds with a significant degree of covalency. Full structural relaxation can result in the opening real gaps on the place of the existing pseudogaps or in a widening of existing gaps.[8]

The final DOS for relaxed structures were evaluated using a the tight-binding linear-muffin-tin-orbital method[83] (TB-LMTO) to enable a very dense Brillouin zone (BZ) sampling necessary for resolving the fine structure of the DOS. This is necessary for excluding the possibility that states located in a small part of the BZ eventually close the gap. The TB-LMTO calculations also provide a decomposition of the electronic DOS into local and angular-momentum-decomposed components.

V. MECHANISM OF SEMICONDUCTING BAND-GAP FORMATION

In this section we show that in Al-Pd-Re quasicrystals specific local bonding configurations form a three-dimensional network of chains of Al-TM bonds extending along the twofold symmetry axes. The topology of this network is instrumental in promoting the formation of a narrow gap in the electronic spectrum. In addition, along these chains strong and weak bonds alternate, and bond alternation further promotes gap formation.

For the actual electronic-structure calculations we are naturally limited to the investigation of finite, not too large unit cells and hence to approximants to quasicrystals only. In our previous studies[60,84] we have demonstrated semiconducting behavior of several quasicrystalline approximants ranging from the smallest 0/1 to the 2/1 approximant. The atomic structure of quasicrystalline approximants is defined in 6D space. In real space the approximants have $P2_13$ (No. 198) symmetry. Out of all cubic space groups, $P2_13$ has the lowest point-group symmetry for the atomic sites: sites with multiplicity 12 have no symmetry at all; sites with multiplicity 4 have trigonal symmetry (point group 3). The atomic structure in real space is thus very complex. In our previous paper[60] we have emphasized that the formation of covalent bonds between Al and TM atoms plays an important role in band-gap formation. The *B*20 structure may be viewed as the lowest (0/1) member in the hierarchy of quasicrystalline approximants. The understanding of the band-gap formation in the *B*20 compounds has proven to be very helpful also for understanding of the band-gap formation in larger approximants to the *F*-type quasicrystals. In Sec. V C we shall demonstrate that the mechanism of band-gap, formation in higher approximants is essentially the same as in the lowest 0/1 approximant—i.e., in FeSi(*B*20). Before describing the mechanism of band-gap formation in *B*20 compounds in detail, it is necessary to discuss the role of hybridization effects and to introduce the notion of a *topological band-gap*. The meaning and importance of this specific type of band-gap is demonstrated at the example of 1/1-Al-Pd-Re.

A. Electronic structure of 1/1-Al-Pd-Re and topological band-gap

The formation of band-gaps or deep pseudogaps in the electronic spectrum of crystals is mostly discussed in terms

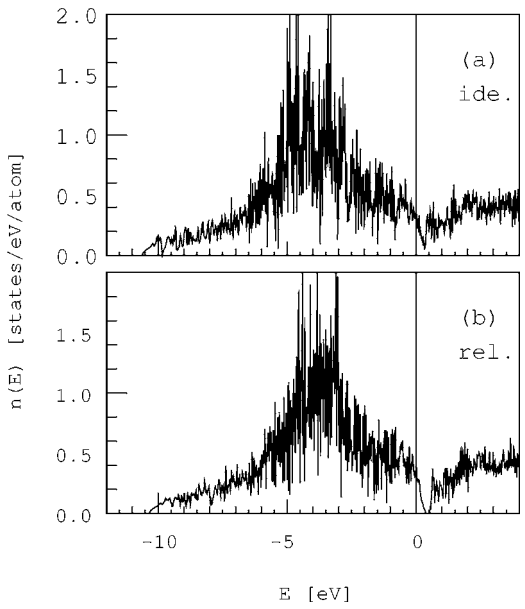

FIG. 1. Total electronic density of states (DOS) of a 1/1 approximant to *i*-Al-Pd-Re with the composition $Al_{88}Pd_{32}Re_8$ (128 atoms per unit cell) for a model with ideal coordinates of atoms as obtained by the 6D projection (a) and for a model with coordinates of atoms relaxed by interatomic forces (b). After the relaxation a deep pseudogap in the DOS changed to a real band-gap at ≈0.35 eV above the Fermi level.

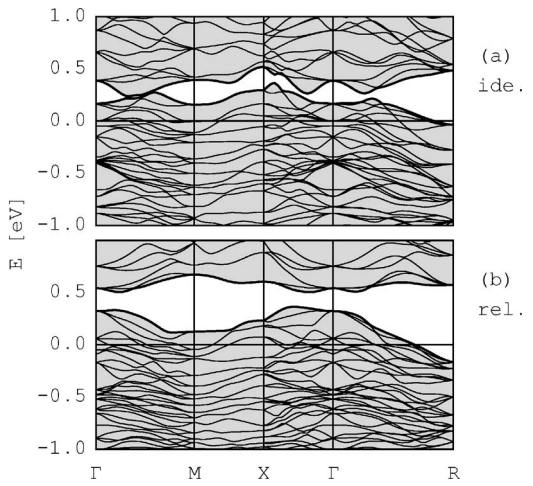

FIG. 2. The band structure a 1/1 approximant to *i*-Al-Pd-Re in an interval ±1 eV around the Fermi level. The individual energy bands are multiply connected in high-symmetry points of the Brillouin zone with one exception: the connected bands are separated just between the 324th and 325th bands—i.e., at the band filling of 648 electrons. The positions of the bands corresponding to the band filling 648 electrons are marked by thicker lines. The overall structure of the bands has "spaghetti"-like character, typical for quasicrystalline approximants.

of hybridization effects. Hybridization also plays an important role in the case of quasicrystalline approximants. Figure 1 shows the DOS of a 1/1 approximant to Al-Pd-Re with composition $Al_{88}Pd_{32}Re_8$ (128 atoms per unit cell) for a model with ideal coordinates of atoms, as obtained by 6D projection (a), and for a model with coordinates of atoms relaxed under influence of the interatomic forces (b). After relaxation the deep pseudogap in the DOS just above E_F becomes a real band-gap at ≈0.35 eV above the Fermi level. The position of the gap corresponds to a band filling of 648 electrons. Figure 2 presents the corresponding band structure in the interval ±1 eV around the Fermi level. The bands corresponding to the highest occupied and lowest empty eigenstates are marked by thicker lines. Investigation of the band structure leads to the following important observations.

(i) The individual energy bands are multiply connected at high-symmetry points of the Brillouin zone: Γ (0,0,0), M (0.5,0.5,0), X (0.5,0,0), and R (0.5,0.5,0.5). Bands are doubly degenerate on the surface of the BZ—e.g., along MX. This double degeneracy results from the nonsymmorphic character of the $P2_13$ space group. The existence of nonprimitive translations related to the 2_1 screw axis leads to the "sticking together" of the bands on the zone surface.[85,86] The twofold or threefold degeneracies at the Γ point are related to the cubic symmetry of the approximant. In addition, one observes an extensive fourfold degeneracy of the bands at the R point, which is again a consequence of the nonsymmorphic $P2_13$ symmetry which leads to a higher degree of degeneracy at the Γ point. The connectivity of the energy bands at high-symmetry points and on the zone surface ensures that for any energy there exist several eigenstates with this energy. The topology of the connected energy bands thus leads to a continuous density of states without any gaps.

(ii) The topology of the connected bands exhibits one exception from this picture. The band complex is disconnected at a band filling of 648 electrons—i.e., between the 324th and 325th bands. The splitting of the band complex exists also for a structure with nonrelaxed atomic positions, but it is substantially larger for the relaxed structure; see Fig. 2(b). For energies between the upper edge of the 324th band and the lower edge of the 325th band there are no states and thus a band-gap in the DOS appears; see Fig. 1(b). In the case of a model with idealized coordinates the bands are disconnected, but the dispersion of the bands between the high-symmetry points—e.g., along the ΓM and XΓ paths—closes a possible gap.

In our previous work[60] we have analyzed the changes in the atomic and electronic structure caused by the structural relaxation. The interatomic distances between Al and TM atoms become shorter and Al-TM bonds of enhanced covalency are formed. In another language these processes correspond to an enhanced hybridization.[87,88] In reciprocal space the bands calculated for idealized coordinates show strong dispersion and almost intersect between high-symmetry points as is seen, e.g., along ΓM in Fig. 2(a). In the relaxed structure the increased hybridization of bands leads to strong repulsion of these bands and thus to their clear separation. In real space s,p orbitals on Al and s,d orbitals on TM atoms form hybrids oriented along the Al-TM bonds. Hybridization thus plays an important role in the formation of a band-gap in the electronic spectrum of quasicrystalline approximants. However, hybridization and enhanced covalency of bonding are frequently observed also in the electronic structure of many crystalline Al-TM compounds, but band-gap formation is observed only for certain crystal structures (we refer to

our recent work on binary and ternary crystalline dialuminides[8,9]). What is still missing is the criterion for the topological separation of the multiply connected bands at a certain band filling, which in cooperation with the hybridization leads to the existence of a true band-gap in the electronic structure. In our work on the crystalline dialuminides we have emphasized the importance of a low site symmetry. For high site symmetry at the TM sites, the *d* orbitals split into different manifolds which form different types of hybrids with the Al orbitals. Although bonding-antibonding gaps may be formed for each group of hybrids, they will not necessarily overlap and the systems will remain metallic. At low site symmetry, all atomic orbitals contribute to the bonding hybrids and there will be only one type of bonding-antibonding gap.

To discuss this topic it is useful to introduce the notion of a *topological band-gap*. In Fig. 2(a) the energy bands are disconnected at certain band filling. Although in this case there is not necessarily a real gap in the electronic spectrum, it is useful to distinguish these separated bands from the other multiply connected bands. We shall say that between these separated bands a topological band-gap is formed. The existence of a topological band-gap thus does not necessarily mean a true gap in the spectrum but apparently it is a prerequisite for the existence of a true band-gap.

We shall show that the existence of the topological band-gap in quasicrystalline approximants has its origin in a network of linear chains of Al-TM bonds. As already noted above to analyze in detail the complex picture of bonds between 128 atoms of the 1/1 approximant is extremely difficult. It is therefore useful to start a detailed analysis with the lowest 0/1 approximant with eight atoms per unit cell. This study we present in Sec. V B. In Sec. V C we shall demonstrate that in larger approximants the mechanism for the band-gap formation is completely analogous.

B. Gap formation in *B*20 phases

The *B*20 structure has $P2_13$ space-group symmetry generated by a twofold screw axis 2_1 and a threefold axis. The Bravais lattice is simple cubic, but the overall point symmetry is tetrahedral. The space group consists of four threefold rotations around ⟨111⟩ directions and three screw axes consisting of a 180° rotation around a cubic axis, followed by a nonprimitive translation by $(\frac{1}{2},\frac{1}{2},0)a$ and combinations thereof. Fe and Si are located at Wyckoff positions (4*a*) with coordinates (u,u,u), $(u+0.5,0.5-u,-u)$, $(-u,0.5+u,0.5-u)$, and $(0.5-u,-u,0.5+u)$. The point symmetry at the Fe and Si sites is C_3—i.e., a threefold rotation about an appropriate axis. The values of the internal coordinates are[28] $u(\mathrm{Fe})=0.1358$ and $u(\mathrm{Si})=0.844$; the lattice parameter is $a=4.489$ Å.

Compounds obtained from FeSi by replacing Fe and Si by isoelectronic elements are also semiconductors.[89] RuSi exhibits a gap of 0.4 eV,[90] and FeGe is a narrow-gap semiconductor[91] with a gap of 10 meV. The stability of the *B*20 structure and the existence of a bonding-antibonding gap is not restricted to compounds formed by Fe-group metals and group-IV elements. We have also mentioned that all

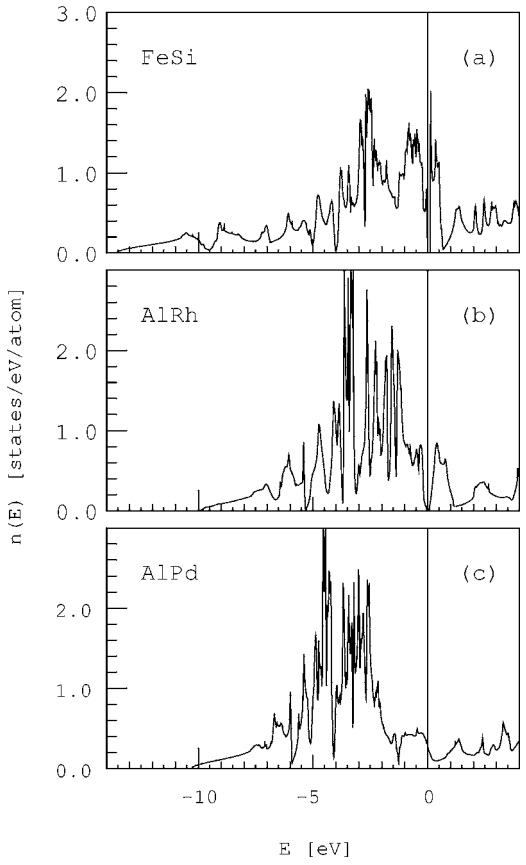

FIG. 3. The DOS of three compounds with the *B*20 structure: (a) FeSi, (b) AlRh, and (c) AlPd: cf. Fig. 4.

monosilicides of Cr, Mn, Fe, and Co adopt the *B*20 structure[25] and show gaps or pseudogaps at a band filling corresponding to FeSi.[23,26,92] Some TM-aluminides also crystallize in the *B*20 structure. However, it is interesting that AlRh (isoelectronic to FeSi) adopts the *B*2 rather than the *B*20 structure, whereas AlPd has a stable *B*20 phase, with a deep pseudogap below and not at the Fermi level.[93]

In Fig. 3 the DOS of three compounds with the *B*20 structure is shown. Figure 3(a) shows the DOS of FeSi.[94] At the Fermi level a narrow real gap in the electronic spectrum is observed. Figure 3(b) shows the DOS of AlRh in the *B*20 structure. This is a hypothetical structure as the stable AlRh compound exists in the *B*2 structure. Nevertheless, for an understanding of the mechanism of the band-gap formation in Al-*M* quasicrystals it is essential to also consider this hypothetical compound. One observes that this compound also exhibits a gap (although of almost zero width) at the Fermi level. The band filling is the same as for FeSi, six electrons per atom. Figure 3(c) shows the DOS of AlPd in the *B*20 structure. This is a stable phase. Pd is a group-12 transition metal; the band filling of the AlPd compound is 6.5 electrons per atom. There is no band-gap or a pseudogap in the DOS at the Fermi level, but one observes a dip in the DOS ≈1.2 eV below the Fermi level. It is the energy corresponding just to a band-filling 6 electrons per atom.

The band structure of FeSi and other *B*20-type compounds has already been discussed in some detail in the literature.[18,20–23] The lowest grouping of bands (∼−13 to

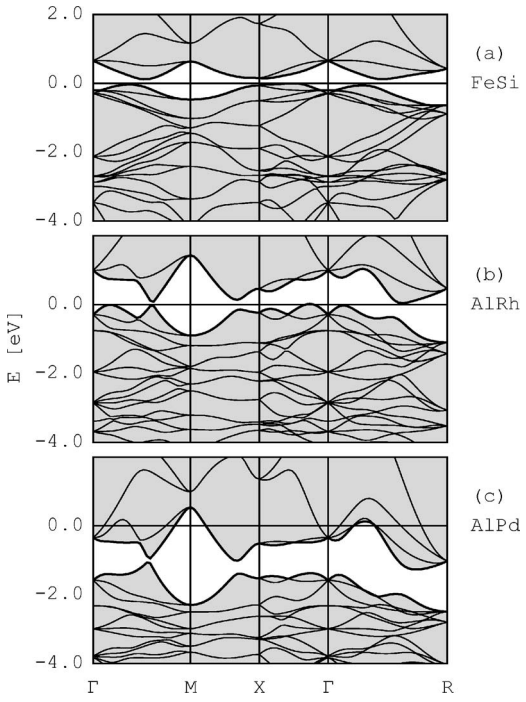

FIG. 4. The band structure around the Fermi level of three compounds with the $B20$ structure: (a) FeSi, (b) AlRh, and (c) AlPd. The overall structure of the bands is similar to that observed in Fig. 2(b) of the Al-Pd-Re 1/1 approximant. Also here the individual energy bands are multiply connected in high-symmetry points of the Brillouin zone with one exception at the band filling of 48 electrons. Dispersion of the bands completely closes a band-gap in AlPd; in AlRh, the band-gap is also closed, however only marginally.

−6 eV) derives from Si *s* states. The hybridization of Fe *d* and Si *p* leads to the formation of a valence-band complex extending from ~ −6 to +6 eV, and contributions from Fe *d* states dominate around E_F, whereas states near the bottom and top of this band complex have strongly mixed Fe-*d*—Si-*p* character. Figure 4 shows the band structure of the three compounds around the Fermi level. This representation emphasizes the similarity of the electronic structure of the $B20$ phases with that of 1/1-Al-Pd-Re due to the same nonsymmorphic space group: As a consequence of the space-group symmetry, energy bands are degenerate and hence multiply connected at high-symmetry points of the Brillouin zone, with one exception: the bands are disconnected just between the 24th and 25th bands—i.e., at a band filling of 48 electrons/cell. In the case of AlRh two bands along Γ-M almost intersect at one point just at the Fermi level. However, band crossing is forbidden because the eigenstates belonging to the bands have the same symmetry and hybridization leads to a repulsion of the bands also at this point. The same is also observed for the other two compounds AlPd and FeSi. Although the energy difference between eigenstates at the high-symmetry points is relatively modest for FeSi, only in this system does a clear nonzero band-gap exist. Dispersion of the bands completely closes the band-gap in AlPd; in AlRh, a very narrow band-gap persists.

Figures 3 and 4 demonstrate that the origin of the band-gap in FeSi is structure induced. The existence of a gap depends on two main features: (i) Bands limiting the gap must be disconnected at the high-symmetry points, and degeneracies of the eigenstates at these points must be lifted due to a low symmetry of the atomic positions. (ii) The eigenstates of the two bands on both sides of the gap must have the same symmetry such that band crossing is forbidden.

We have already mentioned two important structural relationships of the $B20$ structure, with the $B1$ structure and with the "ideal $B20$" structure representing a low-order approximant to the icosahedral quasicrystal. Both relationships are important for understanding the physical mechanism leading to the formation of a band-gap. The $B20$ structure can be viewed as a distorted NaCl lattice. For the parameters $u(\mathrm{Fe})=0.25$ and $u(\mathrm{Si})=0.75$, the unit cell of the $B20$ structure is identical to a supercell of the NaCl structure. The transformation from $B1$ to $B20$ structure involves two steps. (i) The multiplication of the unit cell. In terms of the band structure, this means that the $B1$ zone boundary X point is folded onto the $B20$ zone center, leading to an increased degeneracy (from 2 to 6) of states close to E_F. (ii) Fe and Si atoms are displaced from their positions in the $B1$ structure. This reduces the space-group symmetry (and hence the degree of degeneracy at high-symmetry points) and introduces interactions between states that are noninteracting in the $B1$ structure.

This observation is important for understanding the origin of a band-gap. Figure 5 shows the evolution of the band structure of FeSi in dependence on the u parameter. Part (a) corresponds to the undistorted rocksalt structure with $u=0.25$ for Fe atoms; for Si atoms, this parameter is set to $1-u$ [the condition $u(\mathrm{Si})=1-u(\mathrm{Fe})$ leads to the same bond length for all Fe-Si bonds], part (b) a slightly distorted structure with $u=0.225$, and the last part (c) corresponds to the value $u=0.154$ defining the "ideal $B20$" structure according to Vočadlo *et al.*[27] and Dmitrienko.[29] Figure 5(a) shows that in the undistorted NaCl lattice the bands are multiply degenerate at Γ and X. In a slightly distorted lattice [Fig. 5(b)] this degeneracy is partially removed and the bands are disconnected. No band-gap exists because the hybridization gap along Γ-M is too narrow. In the ideal $B20$ lattice [Fig. 5(c)] the structure-induced gaps at the high-symmetry point and the hybridization gaps along off-symmetry lines become aligned on the energy scale and a real gap is opened. Whether the topological band-gap also becomes a real gap depends, of course, on the dispersion of the bands and on the strength of the hybridization. The gaps in the high-symmetry points and the hybridization gaps have to be properly aligned to overlap. While for FeSi the gaps overlap, for AlPd [Fig. 3(c)] the gaps are not aligned and hence a real gap is not formed. It should be emphasized that the displacements necessary to form the $B20$ from the reference $B1$ structure are large; in the $B1$ lattice, each Fe atom has 6 Si neighbors at ~2.25 Å and 12 Fe neighbors at ~3.18 Å; in the ideal $B20$ structure, Fe has 7 Si neighbors at ~2.41 Å plus 6 Fe neighbors at ~2.75 Å.

We note that seven equidistant neighbors exist only in the ideal $B20$ structure. For a $B20$ structure with the parameter $u(\mathrm{Fe})$ larger (smaller) than the value $1/(4\tau)$ the distance of one of these seven neighbors is larger (smaller) than the

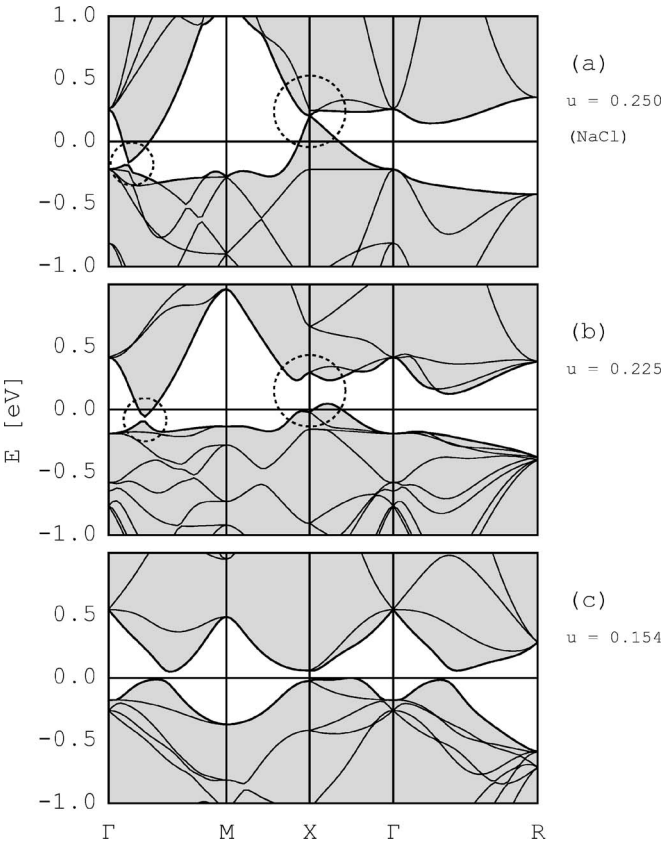

FIG. 5. The $B20$ structure can be viewed as a distorted NaCl lattice. For the parameter $u=0.25$ for Fe and $1-u$ Si the $B20$ is identical to the highly symmetric rocksalt structure. The three panels show the evolution of the band structure of FeSi in dependence on the u parameter: (a) corresponds to the undistorted rocksalt structure with $u=0.25$, (b) corresponds to a slightly distorted structure with $u=0.225$, and (c) corresponds to the value $u=0.15$ which corresponds to the "ideal $B20$" in which each atom is surrounded by seven equidistant neighbors of the opposite kind. In the real $B20$ structure the condition $u(\mathrm{Si})=1-u(\mathrm{Fe})$ is relaxed, cf. text.

other six equidistant neighbors. In Sec. I we have shown that the ideal $B20$ structure can be interpreted as a tiling of prolate and oblate rhombohedra with edges oriented along the threefold- symmetry axes (yellow sticks[30]). Six out of the seven equidistant neighbors form edges of the tiling; the remaining seventh neighbor is a body diagonal of the oblate rhombohedron. In the limiting case of the $B1$ structure the shape of both prolate and oblate rhombohedra becomes a cube. Along the deformation path $B1\rightarrow B20$, where the parameter $u(\mathrm{Fe})$ varies between $1/4$ and $1/(4\tau)$ the cubic structure collapses to a tiling of prolate and oblate rhombohedra. The ideal $B20$ structure can be considered as a special case where the body diagonal of the oblate rhombohedron is just as long as the edges of the tiling. It can be also considered as a limiting case as for smaller values of the parameter $u(\mathrm{Fe})$ one would get unphysically short interatomic distances in the structure. The interaction of the central Fe atom with the seventh nearest neighbor thus prevents further deformation of the rhombohedral tiles and stabilizes the structure (in an analogy to the diagonal fixing elements in, e.g., civil engineering constructions).

The $B1$-$B20$ structural energy difference is about 1.4 eV/formula unit.[18,20] Much smaller (~0.1 eV/formula unit[20,22]) is the structural energy difference with respect to the $B2$ structure, to which the $B20$ phase is predicted to transform under pressure.[20,22,27] In fact, the $B1$ structure was found to correspond to a saddle point on the potential-energy surface along the Bain path relating the $B20$ and $B2$ structures.[20]

The remaining difference between the ideal $B20$ structure with $u(\mathrm{Fe})=1/(4\tau)\sim 0.154$ and $u(\mathrm{Si})=1-u(\mathrm{Fe})$ also leads to an interesting observation. For these coordinates each atom has seven equidistant neighbors of the opposite kind. *Ab initio* optimization of the $B20$ structure of FeSi leads to internal coordinates of $u(\mathrm{Fe})=0.136$, $u(\mathrm{Si})=0.844$, and a lattice constant of $a=4.469$ Å, in excellent agreement with experiment [$u(\mathrm{Fe})=0.1358$, $u(\mathrm{Si})=0.844$, and $a=4.489$ Å)].[28] The relaxation from the ideal $B20$ structure splits the shell of seven nearest neighbors at 2.41 Å into one at 2.27 Å (lying along a [111] direction), three at 2.35 Å and three at 2.52 Å. The structural energy difference between the ideal and relaxed $B20$ structures is 0.128 eV/formula unit (Ref. 22) — i.e., slightly larger than the $B2$-$B20$ energy difference. The relaxation with respect to the "ideal" structure is hence essential for stabilizing the $B20$ relative the $B2$ phase. The effect of the distortion of the $B20$ structure on the chemical bonding is illustrated in Fig. 6 which shows the different electron densities in $B20$-type FeSi, AlRh, and AlPd in a plane containing chains of TM and (Si, Al) atoms. This analysis demonstrates that the chains are dimerized, they contain alternating strong and weak TM-(Si, Al) bonds, and the strength of the bonds is visualized by the enhancement of the electron density at the midpoint between the atoms. For all three compounds FeSi (a), AlRh (b), and AlPd (c)—i.e., independent of the degree of band filling—one observes alternating strong and weak bonds. The bond lengths also reflect the alternant bond strength; the stronger Al-Rh bond measures 2.52 Å, the weaker one 2.62 Å, in this case $u(\mathrm{Al})\neq[1-u(\mathrm{Rh})]$. From Fig. 6 it is seen that the difference between strong and weak bonds is largest for FeSi and smallest for AlPd. The pairing-type distortions of the chains of equidistant atoms of the ideal $B20$ structure lead to a stronger Fe-s–Si-p hybridization and further to a slight widening of the gaps. This effect is quite modest for FeSi and the $B20$-type monoaluminides, but it is of decisive importance for gap formation in the quasicrystals.

Figure 7 shows a projection of the $B20$ crystal along a direction slightly off the (010) axis. Chains of alternating TM and Si(Al) atoms extend along the Cartesian axes. One TM-Si(Al) nearest-neighbor bond (dotted line) is oriented along the [111] axes. Together, these chains form a complex three-dimensional network. Within this network each TM atom has seven nearest neighbors. Three neighboring Si(Al) atoms are bonded strongly, three weakly. The remaining seventh neighbor has a stabilizing role. The characteristic bonding configurations in the $B20$ structure are presented in Fig. 8. The dimerized linear chains of the alternating Si(Al) and TM atoms intersect at TM atoms. The bonding configuration around a TM atom consists of three strong and three weak bonds. The seventh neighbor does not belong to the chain topology, and therefore it is not shown.

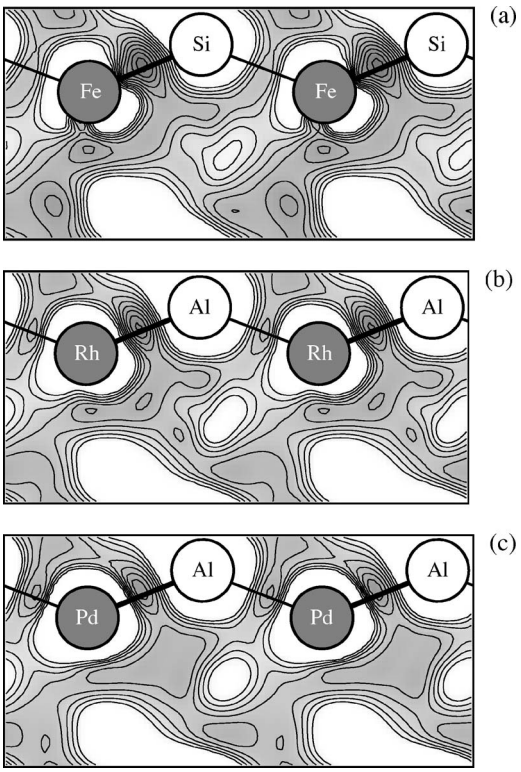

FIG. 6. The contour plot shows a differential charge density distribution in three compounds with the *B*20 structure: (a) FeSi, (b) AlRh, and (c) AlPd. For all three compounds one observes alternating strong and weak bonds. The strength of the bonds manifests itself in an enhancement of the charge density at the midpoint between atoms. The figure demonstrates a dimerization of chains of atoms. Linear chains of alternating strong and weak (Si, Al)-TM bonds are marked explicitly. The interatomic distances between atoms also alternate, cf. text.

The origin of the band-gap in the FeSi structure can be also understood via a band-counting scheme. Out of the Fe *sd* and Si *sp* orbital 40 bands can be formed. The Fe-Si bonds are formed by Fe-sd^4–Si-p^3 hybrids, altogether producing 32 bands. Fe *d* orbital perpendicular to the (111) direction does not contribute to the bonding. Hence we have the following picture: (i) 4 Si *s* bands at low energy (occupied), (ii) 4 nonbonding Fe *d*(perp.) bands, occupied, (iii) 16 occupied bonding Fe-sd^4–Si-p^3 bands, making altogether 24 occupied bands, and (iv) 16 empty antibonding Fe-sd^4–Si-p^3 bands, completing the complex of 40 bands. Hence the mechanism leading to the gap formation is the bonding-antibonding splitting in the Fe-*sd*–Si-*p* band complex.

C. Linear chains of Al-TM bonds in approximants to *i*-Al-Pd-Re

The structure of the *i*-Al-Pd-Mn(Re) quasicrystal has been studied intensively and now is one of the best understood quasicrystalline structures. The structure can be interpreted in terms of pseudo-Mackay and Bergman-type clusters.[64,74,75,95–97] It is relevant to note that the "Mackay" and "Bergman" clusters in *i*-Al-Pd-Mn are a little different from those encountered in various complex intermetallic

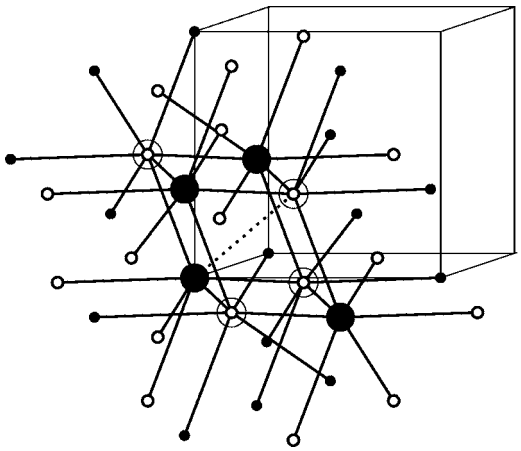

FIG. 7. A projection of the *B*20 structure along a direction slightly of the (010) axis; Solid circles: Fe atoms, Open circles: Si atoms. The structure can be understood as a tiling of two kinds of rhombohedra: prolate and oblate. An oblate rhombohedron is marked explicitly by a larger size of the Fe and Si atoms; the prolate rhombohedron is for simplicity not marked. Each Fe atom has seven neighbors, and six bonds are edges of the tiling; the seventh is the body diagonal of the oblate rhombohedron (dashed line). Chains of nearest-neighbor Fe-Si bonds running along the Cartesian axes can be recognized. In the ideal *B*20 structure all bonds along the chains have the same length; in the real *B*20 structure strong (short) and weak (long) bonds alternate.

crystalline structures. Instead of using the term pseudo-Mackay or pseudo-Bergman we shall, in agreement with Gratias *et al.*,[97] call the clusters the *M* and *B* clusters. Each bc site of the 6D structure of *i*-Al-Pd-Mn(Re) is a center of a *B* cluster, with a Pd atom in the center. The *M* clusters are centered by Mn(Re) atoms. One of the most peculiar features of the structure of *i*-Al-Pd-Mn(Re) is the low coordination of the first atomic shell of the *M* cluster. Seven atoms occupy vertices of a small dodecahedron, but their spatial arrangement around the central Mn(Re) atom is irregular with respect to icosahedral symmetry. This is identical to the sevenfold coordination polyhedron in the ideal *B*20 structure. We note that the local environment in the *i*-Al-Pd-Mn quasicrystals has been discussed also by Quandt and Elser.[78]

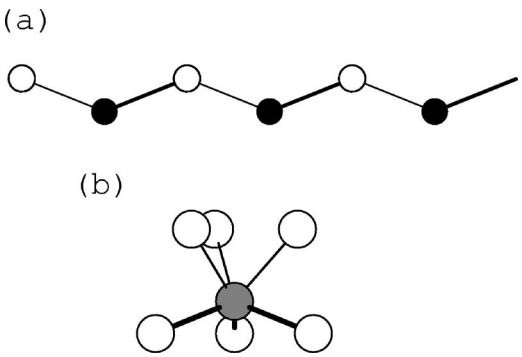

FIG. 8. Bonding configurations in the *B*20 structure: (a) dimerized linear chain of alternating Al/Si (open circles) and TM atoms (solid circles) and (b) three-dimensional bonding configuration of around an individual TM atom, cf. text.

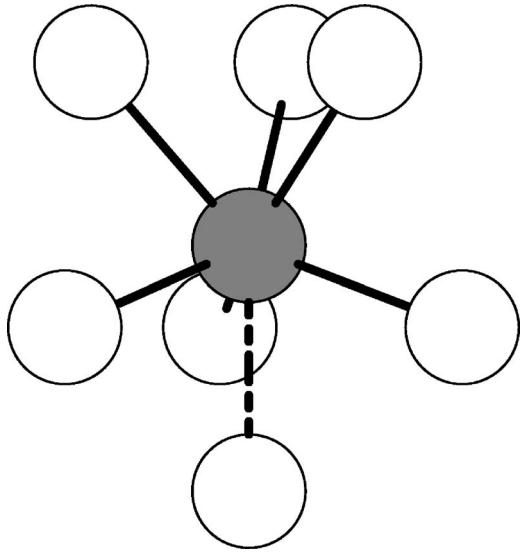

FIG. 9. A bonding configuration in the center of the *M* cluster. The central Re atom is covalently bonded with six (solid lines) out of seven neighboring Al atoms and forms a bonding configuration the same as that in the *B*20 structure; see Fig. 8(b).

Inspection of the three-dimensional charge density distribution in the 1/1 and 2/1 Al-Pd-Re approximants shows that the bonding configurations identified in the *B*20 structure (see Fig. 7) exist also in these approximants. They are precisely the bonding configuration in the low-coordinated centers of the *M* clusters; see Fig. 9. In both structures there are seven neighbors around a TM atom. Six out of seven neighbors of the central Re atom in the *M* cluster form the bonding configuration presented in Fig. 7. Three of the bonds exhibit strong covalency; three bonds are weak. In addition there is a weak bond to the remaining seventh neighbor of the central atom. The bonding configuration has threefold symmetry, and all individual Al-Re bonds are oriented along threefold axes. In three-dimensional representations of the charge density distribution the three strong Al-Re bonds can be well recognized as a characteristic triplet of covalent bonds.

The centers of the *M* clusters are not the only sites in the quasicrystalline approximants where the sixfold bonding configurations are observed. The other sites are at the surface of the *B* clusters. Figure 10 shows a view on the *B* cluster. The outer shell of the *B* cluster is formed by an icosahedron of Al atoms and a dodecahedron of TM atoms. All bonds on the surface are oriented along threefold axes, which we find to be favorable for covalent bonding. If Al-TM bonds exhibit enhanced covalency, the bonding distance becomes shorter. In an *i*-Al-Pd-Mn quasicrystal the length of the quasilattice constant is a_q=4.56 Å. In an ideal structure the shortest bond is oriented along a threefold axis, and its length is $0.5628a_q$=2.57 Å, while the shortest bonds along the fivefold and twofold axes are $0.6180a_q$=2.82 Å and $0.6498a_q$ =2.96 Å, respectively.

The center of the *B* cluster is occupied by a Pd atom. The neighboring Al atoms are located at fivefold vertices—i.e., at 2.82 Å from the center. This distance is already too large for covalent bonding. The TM atoms are located at threefold

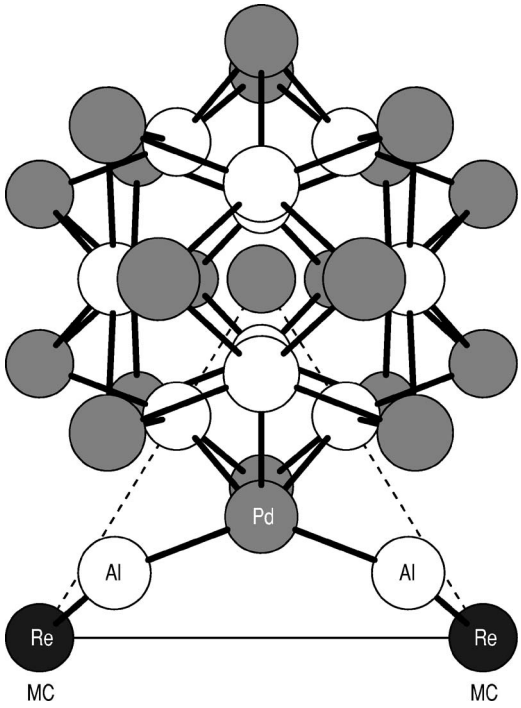

FIG. 10. The upper part shows a view of the *B* cluster. The outer shell of the *B* cluster is formed by an icosahedron of Al atoms (white spheres) and a dodecahedron of Pd atoms (gray spheres). The center of the *B* cluster is occupied by a Pd atom. All bonds on the surface are Al-TM bonds and oriented along threefold axes (thick line segments between spheres). Each TM atom on the surface of the *B* cluster is bonded to three Al atoms on the surface, forming a part of the sixfold bonding configuration as presented in Fig. 8(b). A *B* cluster can be linked with *M* clusters along the fivefold axis (dashed lines). Two centers of the neighboring *M* clusters occupied by Re atoms (dark circles) are explicitly shown in the lower part of figure. The centers of *M* clusters are linked by a chain of alternating Al and Pd atoms. A link between the centers of *M* clusters is oriented along two-fold axes (thin line).

vertices at a nonbonding distance 4.15 Å from the central Pd atom. All bonds on the surface are Al-TM bonds and oriented along three fold axes. On the surface of the *B* cluster one can recognize chains of alternating Al and TM atoms. Each TM atom on the surface of the *B* cluster is bonded to three Al atoms on the surface forming half of the sixfold bonding configuration presented in Fig. 8(b). To see the orientation of the remaining bonds around a TM atom one has to investigate a wider environment of the *B* cluster.

A significant contribution to understanding the real-space atomic structure of *i*-Al-Pd-Mn(Re) has been made by Elser.[95] Elser realized that the Katz-Gratias model of *i*-Al-Pd-Mn can be interpreted as a three-dimensional Penrose tiling with vertices decorated by *B* and *M* clusters. A quasilattice constant of this Penrose tiling measures *a* =7.38 Å; i.e., it is τ=1.618 times larger than a_q. *M* and *B* clusters occupy vertices with opposite parity. On a prolate rhombohedron (PR) four vertices—say, with odd parity—are occupied by *M* clusters and the other four vertices with even parity are occupied by *B* clusters. *M* and *B* clusters are linked along fivefold axes. We also note, that there are existing links

between M and B clusters along threefold axes, located on the long body diagonal of the PR.

A TM atom on the surface of the B cluster can have up to six Al neighbors oriented along threefold axes. Three atoms are on the surface of the B cluster as discussed above, and the other three Al atoms are inside the neighboring M clusters. They are just the Al atoms surrounding the low-coordinated center of the M cluster. The B cluster is linked along fivefold axes with two M clusters forming an acute angle on the face of a PR such that the TM atom has a sixfold bonding configuration with three strong and three weak bonds, the same as presented in Fig. 8(b). Hence the 3+3 bonding configuration can exist in the i-Al-Pd-Mn(Re) quasicrystal at two topologically important sites: at the centers of the M clusters and on the surfaces of the B clusters.

The TM atom on the surface of the B cluster and the Re atom in the center of the M cluster have a common Al neighbor. Two Re atoms at the centers of M clusters decorating the vertices of a PR are linked by a chain of alternating Al and TM atoms: TM- (Re atom at center of M) Al- (first neighbor, one of the low-coordinated shell) TM- (Pd atom at a threefold vertex on the surface of the B cluster) Al- (one of the low-coordinated shell of the second M cluster) TM (Re atom in the center of M). This chain of alternating Al and TM atoms thus consists of five atoms with four bonds between them. It links the centers of two M clusters over a distance of 7.76 Å. This is the length of a short face diagonal of the PR. In units of the edge of the Penrose tiling a the distance is $s=1.051a$. We shall call this a S *segment* of an extended Al-TM chain; see Fig. 11(a). In the Penrose tiling decorated by B and M clusters there is also a τ times larger distance $l=1.701a=12.55$ Å between the M clusters. This is the length of the long face diagonal of a PR. A chain of alternating Al and TM atoms also exists between M clusters separated by the long face diagonal. Such a chain consists of seven atoms with six bonds between them: TM- (Re atom in center of M) Al- (one of the low-coordinated shell) TM- (in a threefold vertex of the surface of the B cluster) Al- (in a fivefold vertex of the B surface) TM- (in a threefold vertex of the surface of the B cluster) Al- (belonging to the inner shell around the center of the second M cluster) TM (Re atom in the center of M). We shall call this an L *segment*; see Fig. 11(b). While the shorter S segment connects centers of M clusters over one TM atom on the surface of a B cluster, the L segment connects centers of M clusters over two TM atoms on the surface of the B cluster.

Although all Al-TM bonds in the chains are oriented along the threefold axes, the overall directions of the S and L segments are oriented along the twofold symmetry axes. The S and L segments decorate faces of rhombohedra as shown in Fig. 12. In one PR four vertices of equal parity are occupied by M clusters, while the other four vertices of opposite parity are occupied by B clusters. The S and L segments of chains of alternating Al-TM bonds connect vertices along face diagonals. Different S or L segments are linked at the vertices of the tile forming together an extended network of infinite chains of alternating Al and TM atoms.

Each Re atom in the center of a M cluster has the local bonding configuration presented in Fig. 9. In each center of a M cluster three perpendicular chains of Al-TM bonds intersect. In a quasicrystalline approximant infinite chains of alternating Al and TM atoms can extend along three perpendicular Cartesian directions, as in the $B20$ structure; see Sec. V B. However, in comparison with the $B20$ structure, the

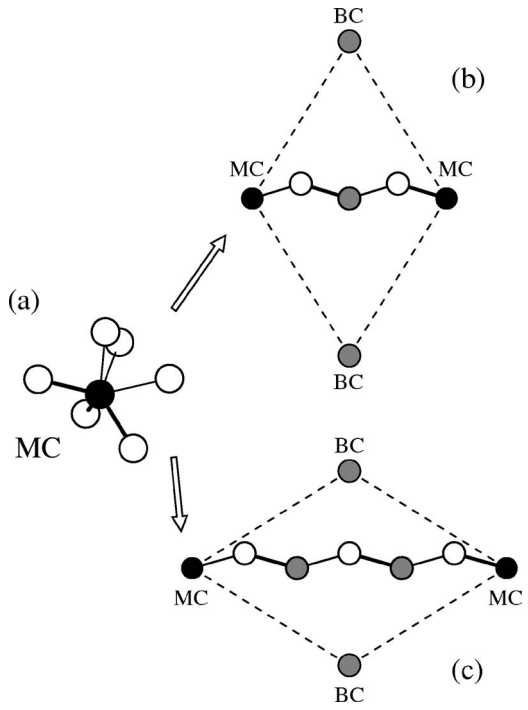

FIG. 11. Chains of alternating Al and TM atoms link the centers of two M clusters (MC) decorating opposite vertices of the rhombohedral faces of the Penrose tiling. Part (a) shows a characteristic bonding configuration of Al atoms (open circles) around the center of the M cluster occupied by a Re atom (black circle). Parts (b) and (c) show the chains of alternating Al and Pd (gray circles) atoms linking the MC along the short (b) and long (c) face diagonal.

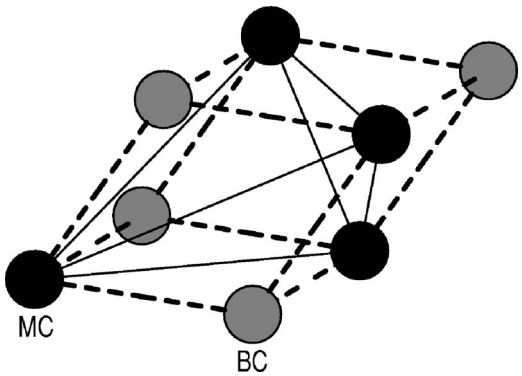

FIG. 12. The real-space structure of i-Al-Pd-Re can be interpreted as a three-dimensional Penrose tiling with vertices decorated by B and M clusters. A quasilattice constant of this Penrose tiling measures 7.38 Å. The centers of B clusters (BCs) are occupied by Pd atoms (gray circles). The centers of the M clusters (MCs) are occupied by Re atoms (black circles). MCs and BCs occupy vertices with opposite parity. MCs and BCs are linked along fivefold axes (dashed lines). Two MCs are linked by chains of alternating Al and TM atoms along the short or long face diagonals (thin lines) of the rhombohedron.

topology of the network of Al-TM chains in the quasicrystalline approximants has another degree of complexity. In icosahedral quasicrystals in addition to 3 twofold symmetry axes along the Cartesian axes there are additional 12 twofold symmetry axes. The linear chains of Al-TM bonds can thus propagate in 15 different twofold symmetry axes intersecting in the *M* clusters. A vertex of the Penrose tiling has on average precisely 6 neighbors at the distance of the short face diagonal.[98] The same holds for the number of neighbors at the distances of the long face diagonal. In one vertex occupied by the *M* cluster on average 6 *S* and *L* segments be linked together. However, in the center of the *M* cluster only 3 chains of Al-TM bonds can intersect. This is not a problem, as the chains can also intersect on the surface of the *M* clusters. An *M* cluster and a *B* cluster linked along the fivefold axis share a part of their surfaces. This part of the *M* cluster around the fivefold axis has thus the same bonding connectivity as shown in Fig. 10. The chains of Al-TM bonds intersect at the Pd atoms at the surface of the cluster. As already noted above the Pd atoms here have a bonding environment similar to that as the Re atom in the center of the *M* cluster; see Fig. 9. One Pd atom on the surface of the *M* cluster can belong to only one or to three chains. As the surface of the *M* cluster is connected on average to 6 chains and 3 chains only intersect at the center, in one Pd atom on the surface of the *M* cluster on average 2 chains intersect.

The existence of chains propagating along the twofold symmetry axes is a special property of the *F*-type icosahedral quasicrystal. While along the fivefold and threefold symmetry axes the inflation rule has τ^3 scaling, along a twofold symmetry axis the scaling is τ. That means if two vertices of the same parity have a distance, say, *s*, then there also exists a vertex at the distance $l=\tau s$. In the Al-Pd-Re quasicrystal thus, there exist one-dimensional Fibonacci chains of Al-TM bonds consisting of a sequence of the *S* and *L* segments.

As we know the chemical composition of the *S* and *L* segments one could attempt to estimate the stoichiometry of the network of the Fibonacci sequence of these segments. Because of the complex topology of the network, this is a very difficult task. However, one can look at this problem from an opposite side. Let us assume that the whole Al-Pd-Re quasicrystal consists of a network of Fibonacci chains of *S* and *L* segments that intersect as indicated above: In each Re atom in the center of the *M* cluster intersect three chains; in each Pd atom on the surface of the *M* cluster intersect (in average) two chains. Then the composition of such a network of the chains would be $Al_{(2+3\tau)}Pd_{(1+2\tau)/2}Re_{(1+\tau)/3}$—i.e., $Al_{0.6962}Pd_{0.2151}Re_{0.0887}$. This composition is surprisingly close to the experimental composition of the *i*-Al-Pd-Mn(Re) quasicrystal [e.g., $Al_{0.705}Pd_{0.21}Mn_{0.085}$ (Ref. 35)]. From the construction of the network of Al-TM chains it is clear that in the structure of the quasicrystal there exist atoms that do not belong to the network of the Al-TM chains. These are, for instance, the Al atoms corresponding to the seventh neighbor around the center of the *M* cluster and the Pd atoms in the centers of the *B* clusters. The fraction of such atoms is only a few percent and can shift the stoichiometry of the structural model even closer to the experimental stoichiometry.

A close relation of the *B*20 structure to the icosahedral quasicrystal has already been mentioned several times and explicitly demonstrated in Sec. I. This relation leads to an alternative view of the *F*-class quasicrystal. It can also be understood as a superstructure of the *B*20 structure. The *B*20 structure is built by the periodic repetition of (yellow-stick[30]) rhombohedral tiles whose odd and even vertices are decorated with TM and Al(Si) atoms, respectively. The icosahedral quasicrystal may be considered a Penrose tiling with golden prolate and oblate rhombohedra, with odd and even vertices occupied by *M* and *B* clusters, respectively. The *M* clusters in the quasicrystal play the role of the TM(Fe) atoms in the *B*20 structure, while the *B* clusters replace the Al(Si) atoms. Chains of Al-TM bonds extend from the center of one *M* cluster over the surface of a neighboring *B* cluster (linked to the *M* cluster along the fivefold axis) to the center of another *M* cluster, in analogy as in the *B*20 structure. A similar superstructure model has recently been proposed in our studies of the $Al_{10}V$ compound.[99] This compound has a complex structure with 176 atoms in the elementary cell which can be interpreted as a superstructure of the cubic Laves phase (structure report symbol *C*15, Cu_2Mg-type) where, e.g., the large Mg atoms are replaced by a Friauf polyhedron consisting of 16 atoms, filing the interstices of a Kagomé network of linear Al-V chains. We also note that an interpretation of the structure of *i*-Al-Pd-Mn quasicrystal in terms of a hierarchy of clusters was also proposed by Janot.[100]

VI. LOCALIZED STATES

In the previous section we argued that in approximants to *i*-Al-Pd-Re and hence also in an infinite *i*-Al-Pd-Re quasicrystal a topological band-gap at the Fermi level can be formed via the same mechanism as in the *B*20 structure. However, a real *i*-Al-Pd-Re quasicrystal is not a perfect semiconductor. This has been verified, e.g., by tunneling spectroscopy measurements[52,53] or photoemission experiments[50,51] presenting evidence for a finite number of states in the gap. In our previous work[60] we have already shown that even a modest degree of substitutional disorder that obviously exists in any real quasicrystalline sample leads to the formation of localized states inside the semiconducting gap.

In the present model we can specify the substitutional disorder more precisely. The main source of a possible chemical disorder is the surface of the *B* cluster. So far we have assumed a decoration of the vertices of the *B* cluster as shown in Fig. 10. We note that the chemical identity of the sites on the surface of the *B* cluster is defined in the KGB model by the details of the interface between the middle Pd shell and the outer Al shell of the "even" occupation domain. In the KGB model this interface has the form of a triacontahedron. In larger approximants one finds that the decoration of the surface of some *B* clusters is not perfect as shown in Fig. 10, and some sites on the pentagonal dodecahedron are occupied by Al atoms, while some icosahedral vertices are occupied by of Pd atoms.

The alternating sequence of Al and TM atoms on the chains can thus be broken by substitutional Al/Pd defects. In our previous paper we have already explicitly demonstrated that such a defect leads to the appearance of localized states

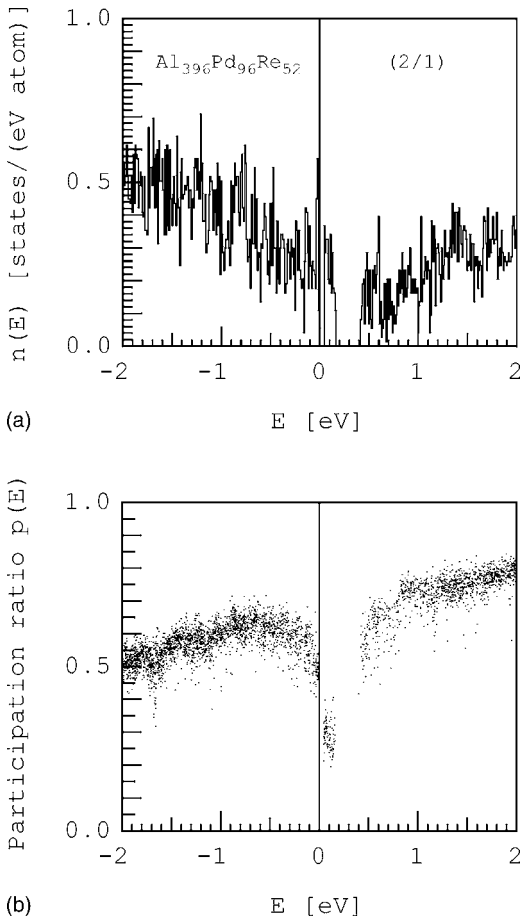

FIG. 13. The total DOS (a) and participation ratio of eigenstates of a 2/1 Al-Pd-Re approximant with the composition of $Al_{72.8}Pd_{17.6}Re_{9.6}$. Only a part of the spectrum around the Fermi level is shown. The model of 2/1 approximant provides both ingredients of the anomalous electronic structure of the *i*-Al-Pd-Re quasicrystal—a band-gap in the spectrum, at or very close to the Fermi level and the localized states. Just at the Fermi level one observes a very narrow gap of width 40 meV. Above the Fermi level in the energy interval 0.04-0.17 eV there is a group of localized states. Another larger band gap of width 0.19 eV extends in the energy interval 0.17–0.36 eV above the Fermi level.

inside the semiconducting band-gap. We note that a possible substitutional disorder between two different TM species has only a minimal effect on the semiconducting gap. The shape of the interface between the inner Re core and middle Pd shell of the even occupation domain in the KGB model is thus from this point of view not so critical.

Figure 13 shows the total DOS (a) and the participation ratio of eigenstates of a 2/1 Al-Pd-Re approximant as obtained from the KGB model. The composition of the model is $Al_{72.8}Pd_{17.6}Re_{9.6}$; i.e., it is already quite close to the composition of *i*-Al-Pd-Re. Our model of the 2/1 approximant provides both ingredients of the anomalous electronic structure of the *i*-Al-Pd-Re quasicrystal—a band-gap in the spectrum, at or very close to the Fermi level, and localized states in the gap. Just at the Fermi level one observes a very narrow (40 meV-wide) gap. Above the Fermi level in the energy interval from 0.04 eV to 0.17 eV we find a group of localized states. Another larger band-gap of width 0.19 eV extends from 0.17 eV to 0.36 eV above the Fermi level.

The localized states in this 2/1 approximant are created by substitutional defects. The structural model of the 2/1 approximant consists of 50 independent Wyckoff positions. We performed several attempts to modify the chemical identity of some sites to get a model with a clean band-gap without the localized states, but our attempts were not successful. If we create a perfect chemical decoration of some *B* cluster, this spoils the decoration of a neighboring *M* cluster. At present we cannot decide whether a "perfect" 2/1 (or higher) approximant, with the correct chemical decoration of all *M* and *B* clusters, is possible. Our experience with structural modeling indicates that a certain degree of chemical disorder seems to be inherent even to an ideal *i*-Al-Pd-Re quasicrystal. It is therefore quite understandable that in more sophisticated models of *i*-Al-Pd-Mn(Re) quasicrystal[77] a substantial part of the sites has mixed chemical occupancies. The idealized KGB model with simple triacontahedral shapes of the internal shells of the occupation domains uniquely determining the chemical identity of the sites thus provides a structural model with a certain minimal degree of the chemical disorder.

The participation ratio of the localized states in the gap shown in Fig. 13 ranges between 0.18 and 0.38, whereas eigenstates on both sides of the gap have participation ratios between 0.5 and 0.8. In our previous work[60] we have shown that the degree of the localization depends on the overlap of the neighboring localized states and hence on the distance between the center of gravity of the localized states in real space. As for periodic approximants the substitutional defects are necessarily periodically repeated, the lattice constant of the approximant sets an upper limit to the distance between localized states and the overlap of the repeated localized states reduces their localization. If the distance between defects is increased, the degree of localization increases and hence the participation ratio scales down with increasing order of the approximants, see Figs. 9 and 10 in Ref. 60.

Figure 14 shows the band structure of the 2/1 Al-Pd-Re approximant. As the space-group symmetry is the same ($P2_13$) for all approximants, the overall picture is the same as for the 0/1 ($B20$) and the 1/1 approximants: threefold degeneracy of eigenstates at Γ, fourfold at R, and "sticking" of pairs of bands over the entire surface of the Brillouin zone. The smaller size of the Brillouin zone of the 2/1 approximant is reflected in a smaller dispersion of the bands. Hence the chance that the "topological" gap at the high-symmetry points and the hybridization gap overlap is greater than in the lower-order approximants. The group of localized states just above the Fermi level exhibits a weak dispersion. We assume that this nonzero dispersion of the localized states is responsible for the residual conductivity $\sigma(0\ \mathrm{K})$ observed in the low-temperature (below 1 K) resistivity measurements[34] of *i*-Al-Pd-Re samples. This small dispersion of localized states gives rise to a nonzero bandwidth of the localized states analogous to the impurity band in heavily doped semiconductors. Considering that the interaction of the localized states decreases with a decreasing disorder this residual conductivity will scale down with the decreasing

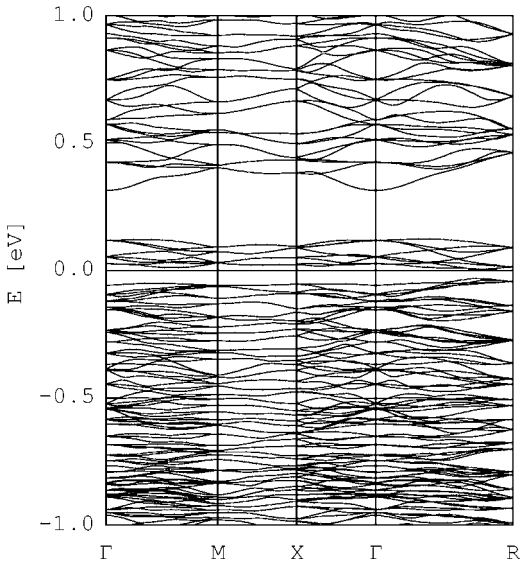

FIG. 14. A band structure of the 2/1 Al-Pd-Re approximant. The overall picture is similar to that of 1/1 approximant; see Fig. 2. A smaller size of the Brillouin zone of the 2/1 approximant is reflected in a smaller dispersion of the bands. A group of the localized states just above the Fermi level exhibits a small dispersion.

disorder, as has been experimentally observed.[47] However, as a minimal substitutional disorder and hence the localized states seem to exist even in a "perfect" quasicrystal this residual conductivity $\sigma(0\ \mathrm{K})$ will be present even in the most perfect (with the highest resistance ratio R) samples of the i-Al-Pd-Re quasicrystal.

VII. DISCUSSION

Our KGB model of the atomic structure of i-Al-Pd-Re provides all ingredients required for understanding the anomalous electronic properties of the quasicrystal: a topologically induced band-gap in the spectrum, at or very close to the Fermi level, and localized states in the gap due to the presence of some intrinsic disorder in the quasicrystalline structure.

We have shown that the origin of the semiconducting band-gap in the electronic spectrum of the i-Al-Pd-Re approximants is essentially the same as in the FeSi ($B20$) structure, which may be considered as the lowest-order (0/1) approximant. All approximants have the same nonsymmorphic space group symmetry $[P2_13(T^4)]$, and in the $B20$ structure as well as in the entire hierarchy of approximants we have identified a three-dimensional network of linear chains of Si(Al)-TM bonds extending along the twofold symmetry directions. Although the overall orientation of the chains is along a twofold axis, the individual Al(Si-TM) bonds are always oriented along a threefold axis, as required by the site symmetry in the $P2_13$ space-group. The valence bands consist of nonbonding Al(Si) s bands, nonbonding Fe d states, and a complex of hybrid TM d Al(Si) p orbitals forming the bonds along the linear chains. The band-gap is formed by the bonding-antibonding splitting of the hybrid orbitals. In an ideal $B20$ structure or in an ideal approximant all bonds along the chain have the same length. Both for the $B20$ phases and for the quasicrystalline approximants, relaxation under the influence of the interatomic forces (calculated via the Hellmann-Feynman theorem) leads to a dimerization of the chains, with alternating strong (short) and weak (long) bonds. The dimerization leads to increased hybridization and tends to widen the topologically induced gap of the ideal structure. For the $B20$ phases, this effect has only a modest influence on the width of the gap, but it is critical for the stabilization of the $B20$ against the competing $B2$ structure. For the quasicrystalline approximants, the dimerization is important for the widening of the hybridization gap and the opening of a real gap, whereas in the ideal structure valence-band maxima and conduction-band minima are located at different off-symmetry points overlap, causing the gap to close. The mechanism leading to the widening of the topological band-gap is similar to, but not identical to the Peierls mechanism.

The chain connecting the centers of neighboring M clusters consists of four individual Al-TM bonds (S segment, linkage across the short face diagonal of a tile) or six Al-TM bonds (L segment, linkage across the long face diagonal of a tile). Considering that the centers of the M clusters are distributed quasiperiodically one gets infinite Fibonacci chains of bonds consisting of S and L segments and extending along twofold symmetry axes.

The origin of the semiconducting band-gap in the i-Al-Pd-Re quasicrystal is in the existence of the linear chains of Al-TM bonds. However, one cannot expect that a real i-Al-Pd-Re quasicrystal is a semiconductor with a clean gap. The fragmentation of the chains by phason defects and particularly by substitutional Al/Pd defects leads to the formation of localized states in the band-gap. The i-Al-Pd-Re quasicrystal thus behaves as a disordered semiconductor. Conduction at very low temperatures proceeds via electron hopping between exponentially localized states. Delahaye *et al.*[35] found that the conductivity of i-Al-Pd-Re follows Mott's VRH conduction law in the temperature range 20–600 mK. This is an experimental confirmation that the i-Al-Pd-Re phase at very low temperature behaves like a disordered semiconductor. Magnetoresistance measurements[34,38] also confirm the VRH mechanism, but the Efros-Shklovskii VRH mechanism incorporating the Coulomb interaction seems to be more appropriate. A complex temperature dependence of the magnetoresistivity has also been reported for FeSi and other $B20$ phases. Jeong and Pickett[23] have pointed out that the nonsymmorphic space group of the $B20$ structure has immediate consequences on the optical and transport properties.

The Al-Pd-Re quasicrystal exhibits the semiconducting behavior if the Fermi level falls into the region of the localized states in the gap. This condition determines a certain narrow range of compositions of samples with semiconducting behavior. The anomalous transport properties were reported for samples with compositions around the $Al_{0.705}Pd_{0.21}Re_{0.085}$ composition. If the composition of a sample is significantly different, as was observed, for instance, for some single-grain samples where the compositions $Al_{0.717}Pd_{0.194}Re_{0.089}$ (Ref. 101) or $Al_{0.735}Pd_{0.171}Re_{0.094}$ (Ref. 102) were reported, the Fermi level falls out of the gap

and the sample will exhibit a metallic conductivity.

The distribution of the localized states in the gap can be quite irregular as is seen in Fig. 13 or in Figs. 7–10 of our previous study.[60] the transport properties of a sample thus depend on the exact position of the Fermi level in the gap. Different samples of the Al-Pd-Re quasicrystal can therefore exhibit different degree of anomalous transport expressed by different values of the resistivity ratio parameter R. Such a behavior is indeed frequently observed.[33,34] It is known[33] that the low-temperature resistivity $\rho(4.2\ \mathrm{K})$ can change by two orders of magnitude for samples of the same nominal composition and prepared in the same way. These experimental facts can be considered as a further indirect support for the explanation of the anomalous transport properties of *i*-Al-Pd-Re quasicrystal by the picture of a disordered semiconductor.

Note added: Recently, a paper by Dolinšek *et al.*[103] came to our attention. In their work, Dolinšek *et al.* proposed a different explanation of the high-resistive behavior of *i*-Al-Pd-Re, based on the comparison of the electrical resistivities of polygrain and single-grain *i*-Al-Pd-Re samples. While the polygrain sample produced in bulk form by casting and annealing exhibited the anomalous transport properties characteristic of a semiconducting material, the resistivity of a single-grain sample showed metalliclike behavior with a low-temperature resistivity of $\rho(4.2\ \mathrm{K})=2.7\mathrm{m}\Omega\,\mathrm{cm}$ only. The authors concluded that the semiconducting behavior of *i*-Al-Pd-Re is not intrinsic, but should be attributed to an extrinsic origin—i.e., to the high porosity of the polygrain samples. The internal surfaces of this granular material are strongly oxidized, leading to the formation of weakly insulating regions in the material. If this explanation is accepted, this would invalidate the conclusions drawn from our theoretical model. However, there are two reasons why we are convinced that this is not the case: (i) The compositions of their polygrain and monocrystalline samples are significantly different. The composition of their single-grain sample for which metallic behavior has been reported is $Al_{0.735}Pd_{0.171}Re_{0.094}$—this is similar to the single-crystalline samples for which Guo *et al.*[101] and Fisher *et al.*[102] ($Al_{0.717}Pd_{0.194}Re_{0.089}$ and $Al_{0.735}Pd_{0.171}Re_{0.094}$, respectively), but significantly different from the asymptotic composition of our model in the quasiperiodic limit ($Al_{0.7073}Pd_{0.2063}Re_{0.0864}$), and differs also from the composition of the samples ($Al_{0.705}Pd_{0.21}Re_{0.085}$) for which, e.g., Delahaye *et al.*[33] and Srinivas *et al.*[34,38] have reported variable-range hopping behavior of the low-temperature conductivity and magnetoresistance as in a disordered semiconductor. The lower content of Pd and the higher concentration of Al and Re in the sample investigated by Dolinsek *et al.* results in a lower electron concentration. In such a case our model predicts that the Fermi level falls below the gap and that the samples exhibit metallic behavior. Hence at this point there is no disagreement between theory and experiment. (ii) The porosity of the polygrain sample reported by Dolinsek *et al.* is characteristic of bulk samples prepared by casting and annealing. It does not exist in samples prepared in ribbon form by rapid quenching. However, at the moment no conclusive data on the composition dependence of ribbon-samples *i*-Al-Pd-Re are available—this could indeed provide a stringent test of our theoretical predictions.

ACKNOWLEDGMENTS

We thank M. Mihalkovič for fruitful discussions. This work has been supported by the Austrian Ministry for Education, Science and Art through the Center for Computational Materials Science and by the Austrian Science Funds through the National Research Network "Nanostructures at Surfaces." M. K. also thanks for support given from the Grant Agency for Science of Slovakia (Grant No. 2/5096/25) and from the Agency for Support of Science and Technology (Grant No. APVT-51052702, CEX-Nanosmart).

[1] F. Bloch, Z. Phys. **57**, 545 (1929); A. H. Wilson, Proc. R. Soc. London, Ser. A **133**, 458 (1931).
[2] N. F. Mott, *Metal-Insulator Transitions* (Taylor and Francis, London, 1990); see also G. A. Sawatzky, in *On the Electronic Structure and Related Physical Properties of Transition Metal Compounds*, edited by J. G. Bendorz and K. A. Müller, Springer Series Solid State Sciences Vol. 90 (Springer, Berlin, 1989).
[3] G. Aeppli and Z. Fisk, Comments Condens. Matter Phys. **16**, 155 (1992).
[4] R. Peierls, *Quantum Theory of Solids* (Pergamon, Oxford, 1955).
[5] P. B. Littlewood, Crit. Rev. Solid State Mater. Sci. **11**, 229 (1983).
[6] J. Y. Raty, J. P. Gaspard, R. Ceolin, and R. Bellissent, J. Non-Cryst. Solids **232**, 59 (1998).
[7] D. Nguyen Manh, G. Trambly de Laissardière, J. P. Julien, D. Mayou, and F. Cyrot-Lackmann, Solid State Commun. **82**, 329 (1992).
[8] M. Krajčí and J. Hafner, J. Phys.: Condens. Matter **14**, 5755 (2002).
[9] M. Krajčí and J. Hafner, J. Phys.: Condens. Matter **14**, 7201 (2002).
[10] D. C. Frederickson, S. Lee, R. Hoffmann, and J. Lin, Inorg. Chem. **43**, 6151 (2004).
[11] D. C. Frederickson, S. Lee, and R. Hoffmann, Inorg. Chem. **43**, 6159 (2004).
[12] H. Nowotny, in *The Chemistry of Extended Defects in Nonmetallic Solids*, edited by L. Eyring and M. O'Keefe (North-Holland, Amsterdam, 1970).
[13] V. Jaccarino, G. K. Wertheim, J. H. Wernick, L. R. Walker, and S. Arajs, Phys. Rev. **160**, 476 (1967).
[14] Z. Schlesinger, Z. Fisk, H.-T. Zhang, M. B. Maple, J. F. DiTusa, and G. Aeppli, Phys. Rev. Lett. **71**, 1748 (1993).
[15] L. Degeorgi, M. B. Hunt, H. R. Ott, M. Dressel, B. J. Fenstra, G. Grüner, Z. Fisk, and P. Canfield, Europhys. Lett. **28**, 341 (1994).
[16] C.-H. Park, Z.-X. Shen, A. G. Loeser, D. S. Dessau, D. G. Mandrus, A. Migliori, J. Sarrao, and Z. Fisk, Phys. Rev. B **52**, R16981 (1995).
[17] J. F. DiTusa, K. Friemelt, E. Bucher, G. Aeppli, and A. P.

Ramirez, Phys. Rev. Lett. **78**, 2831 (1997).
[18] L. F. Mattheiss and D. R. Hamann, Phys. Rev. B **47**, 13114 (1993).
[19] T. Jarlborg, Phys. Rev. Lett. **77**, 3693 (1996).
[20] E. G. Moroni, W. Wolf, J. Hafner, and R. Podloucky, Phys. Rev. B **59**, 12860 (1999).
[21] T. Jarlborg, Phys. Rev. B **59**, 15002 (1999).
[22] A. I. Al-Sharif, M. Abu-Jafar, and A. Qteish, J. Phys.: Condens. Matter **13**, 2807 (2001).
[23] T. Jeong and W. E. Pickett, Phys. Rev. B **70**, 075114 (2004).
[24] H. Yamada, K. Terao, and T. Goto, Physica B **344**, 451 (2004).
[25] D. Shinoda and S. Asanabe, J. Phys. Soc. Jpn. **21**, 555 (1966).
[26] O. Nakanishi, A. Yanase, and A. Hasegawa, J. Magn. Magn. Mater. **15**, 879 (1980).
[27] L. Vočadlo, G. D. Price, and I. G. Wood, Acta Crystallogr., Sect. B: Struct. Sci. **55**, 484 (1999).
[28] P. Villars and L. D. Calvert, *Pearson's Handbook of Crystallographic Data for Intermetallic Phases* (American Society for Metals, Metals Park, OH, 1985).
[29] V. E. Dmitrienko, Acta Crystallogr., Sect. A: Found. Crystallogr. **50**, 515 (1994).
[30] see http://www.zometool.com
[31] C. L. Henley, Phys. Rev. B **43**, 993 (1991).
[32] Ö. Rapp, in *Physical Properties of Quasicrystals*, edited by Z. M. Stadnik (Springer, Berlin, 1999), p. 127.
[33] J. Delahaye and C. Berger, Phys. Rev. B **64**, 094203 (2001).
[34] V. Srinivas, M. Rodmar, R. König, S. J. Poon, and Ö. Rapp, Phys. Rev. B **65**, 094206 (2002).
[35] J. Delahaye, J. P. Brison, and C. Berger, Phys. Rev. Lett. **81**, 4204 (1998).
[36] N. F. Mott, J. Non-Cryst. Solids **1**, 1 (1968).
[37] K. H. Chen, T. I. Su, H. C. Fang, S. C. Lee, and S. T. Lin, J. Alloys Compd. **342**, 352 (2002).
[38] V. Srinivas, M. Rodmar, S. J. Poon, and Ö. Rapp, Phys. Rev. B **63**, 172202 (2001).
[39] B. I. Shklovskij and A. L. Efros, *Electronic Properties of Doped Semiconductors*, Solid State Physics Vol. 45 (Springer-Verlag, Berlin, 1984).
[40] Tzung-I Su, C.-R. Wang, S.-T. Lin, and R. Rosenbaum, Phys. Rev. B **66**, 054438 (2002).
[41] T. I. Su, C. R. Wang, S. C. Lee, S. T. Lin, and R. Rosenbaum, J. Alloys Compd. **342**, 389 (2002).
[42] R. Rosenbaum, T. Murphy, B. Brandt, C. R. Wang, Y. L. Zhong, S. W. Wu, S. T. Lin, and J. J. Lin, J. Phys.: Condens. Matter **16**, 821 (2004).
[43] R. Rosenbaum, B. Grushko, and Przepiórzyński, J. Low Temp. Phys. **142**, 101 (2006).
[44] A. E. Karkin, B. N. Goshchitskii, V. I. Voronin, S. J. Poon, V. Srinivas, and Ö. Rapp, Phys. Rev. B **66**, 092203 (2002).
[45] J.-J. Préjean, C. Berger, A. Sulpice, and Y. Calvayrac, Phys. Rev. B **65**, 140203(R) (2002).
[46] C. Berger, J. Delahaye, T. Grenet, T. Schaub, G. Fourcaudot, J.-P. Brison, and J. J. Préjean, Physica B **280**, 262 (2000).
[47] Ö. Rapp, V. Srinivas, P. Nordbald, and S. J. Poon, J. Non-Cryst. Solids **334**, 356 (2004).
[48] F. S. Pierce, Q. Guo, and S. J. Poon, Phys. Rev. Lett. **73**, 2220 (1994).
[49] M. A. Chernikov, A. Bianchi, E. Felder, U. Gubler, and H. R. Ott, Europhys. Lett. **35**, 431 (1996).
[50] X. Wu, S. W. Kycia, C. G. Olson, P. J. Benning, A. I. Goldman, and D. W. Lynch, Phys. Rev. Lett. **75**, 4540 (1995).
[51] Esther Belin-Ferré, J. Non-Cryst. Solids **334**, 323 (2004).
[52] D. N. Davydov, D. Mayou, C. Berger, C. Gignoux, A. Neumann, A. G. M. Jansen, and P. Wyder, Phys. Rev. Lett. **77**, 3173 (1996).
[53] T. Schaub, J. Delahaye, C. Gignoux, C. Berger, G. Fourcaudot, F. Giroud, T. Grenet, and A. G. M. Jansen, J. Non-Cryst. Solids **250**, 874 (1999).
[54] X.-P. Tang, E. A. Hill, S. K. Wonnell, S. J. Poon, and Y. Wu, Phys. Rev. Lett. **79**, 1070 (1997).
[55] T. Fujiwara, T. Mitsui, and S. Yamamoto, Phys. Rev. B **53**, R2910 (1996).
[56] D. Mayou, Phys. Rev. Lett. **85**, 1290 (2000).
[57] F. Triozon, J. Vidal, R. Mosseri, and D. Mayou, Phys. Rev. B **65**, 220202(R) (2002).
[58] T. C. Choy, Phys. Rev. B **35**, 1456 (1987).
[59] M. Krajčí, J. Hafner, and M. Mihalkovič, Phys. Rev. B **65**, 024205 (2001).
[60] M. Krajčí and J. Hafner, Phys. Rev. B **68**, 165202 (2003).
[61] K. Kirihara, T. Nakata, M. Takata, Y. Kubota, E. Nishibori, K. Kimura, and M. Sakata, Phys. Rev. Lett. **85**, 3468 (2000).
[62] K. Kirihara and K. Kimura, Phys. Rev. B **64**, 212201 (2001).
[63] M. Cornier-Quiquandon, A. Quivy, S. Lefebvre, E. Elkaim, G. Heger, A. Katz, and D. Gratias, Phys. Rev. B **44**, 2071 (1991).
[64] A. Katz and D. Gratias, J. Non-Cryst. Solids **153**, 187 (1993).
[65] M. Boudard, M. de Boissieu, C. Janot, G. Heger, C. Beeli, H.-U. Nissen, H. Vincent, R. Ibberson, M. Audier, and J. M. Dubois, J. Phys.: Condens. Matter **4**, 10149 (1992).
[66] M. de Boissieu, P. Stephens, M. Boudard, C. Janot, D. L. Chapman, and M. Audier, J. Phys.: Condens. Matter **6**, 10725 (1994).
[67] M. Krajčí, M. Windisch, J. Hafner, G. Kresse, and M. Mihalkovič, Phys. Rev. B **51**, 17355 (1995).
[68] E. Cockayne, R. Phillips, X. B. Kan, S. C. Moss, J. L. Robertson, T. Ishimasa, and M. Mori, J. Non-Cryst. Solids **153**, 140 (1993).
[69] C. R. Lin, S. T. Lin, C. R. Wang, S. L. Chou, H. E. Horng, J. M. Cheng, Y. D. Yao, and S. C. Lai, J. Phys.: Condens. Matter **9**, 1509 (1997).
[70] L. Barbier, D. Le Floc'h, Y. Calvayrac, and D. Gratias, Phys. Rev. Lett. **88**, 085506 (2002).
[71] G. W. Zhang and Z. M. Stadnik, in *Proceedings of the 5th International Conference on Quasicrystals*, edited by C. Janot and R. Mosseri (World Scientific, Singapore, 1995), p. 552.
[72] M. Krajčí and J. Hafner, Phys. Rev. B **71**, 054202 (2005).
[73] M. Krajčí, J. Hafner, J. Ledieu, and R. McGrath, Phys. Rev. B **73**, 024202 (2006).
[74] Z. Papadopolos, P. Kramer, and W. Liebermeister, in *Proceedings of the International Conference on Aperiodic Crystals*, edited by M. de Boissieu, J.-L. Verger-Gaugry, and R. Currat (World Scientific, Singapore, 1997), p. 173.
[75] P. Kramer, Z. Papadopolos, and W. Liebermeister, in *Proceedings of the 6th International Conference on Quasicrystals*, edited by S. Takeuchi and T. Fujiwara (World Scientific, Singapore, 1998), p. 71.
[76] A. Yamamoto, Acta Crystallogr., Sect. A: Found. Crystallogr. **52**, 509 (1996).
[77] A. Yamamoto, H. Takakura, and A. P. Tsai, Phys. Rev. B **68**, 094201 (2003).
[78] A. Quandt and V. Elser, Phys. Rev. B **61**, 9336 (2000).
[79] E. S. Zijlstra, S. K. Bose, M. Klanjšek, P. Jeglič, and J. Dolinšek, Phys. Rev. B **72**, 174206 (2005).

[80] G. Kresse and J. Furthmüller, Comput. Mater. Sci. **6**, 15 (1996); Phys. Rev. B **54**, 11169 (1996).
[81] G. Kresse and D. Joubert, Phys. Rev. B **59**, 1758 (1999).
[82] J. P. Perdew and Y. Wang, Phys. Rev. B **45**, 13244 (1992).
[83] O. K. Andersen, D. Jepsen, and M. Šob, in *Electronic Band Structure and its Applications*, edited by M. Youssouff (Springer, Berlin, 1987).
[84] M. Krajčí and J. Hafner, Phys. Rev. B **67**, 052201 (2003).
[85] A. König and N. D. Mermin, Proc. Natl. Acad. Sci. U.S.A. **96**, 3502 (1999).
[86] A. König and N. D. Mermin, Am. J. Phys. **68**, 525 (2000).
[87] U. Mizutani, in *The Science of Complex Alloy Phases*, edited by T. B. Massalski and P. E. A. Turchi (TMS, Warrendale, PA, 2005), p. 1.
[88] G. Trambly de Laissardière, D. Nguyen-Manh, and D. Mayou, Prog. Mater. Sci. **50**, 679 (2005).
[89] G. M. He, S. P. Li, and M. C. Huang, Chin. Phys. Lett. **18**, 1389 (2001).
[90] V. Vescoli, L. Degiorgi, B. Buschinger, W. Guth, C. Geibel, and F. Steglich, Solid State Commun. **105**, 367 (1998).
[91] H. Yamada, K. Terao, H. Ohta, and E. Kulatov, Physica B **329**, 1131 (2003).
[92] Y. Imai, M. Mukaida, K. Kobayashi, and T. Tsunoda, Intermetallics **9**, 261 (2001).
[93] D. Nguyen-Manh and D. G. Pettifor, Intermetallics **7**, 1095 (1999).
[94] R. Hoffmann, *Solids and Surfaces: A Chemist's View of Bonding in Extended Structures* (VCH, New York, 1988).
[95] V. Elser, Philos. Mag. B **73**, 641 (1996).
[96] G. Kasner, Z. Papadopolos, P. Kramer, and D. E. Bürgler, Phys. Rev. B **60**, 3899 (1999).
[97] D. Gratias, F. Puyraimond, M. Quiquandon, and A. Katz, Phys. Rev. B **63**, 024202 (2000).
[98] C. L. Henley, Phys. Rev. B **34**, 797 (1986).
[99] M. Jahnátek, M. Krajčí, and J. Hafner, J. Phys.: Condens. Matter **15**, 5675 (2003).
[100] C. Janot, J. Phys.: Condens. Matter **9**, 1493 (1997).
[101] J. Q. Guo, T. J. Sato, E. Abe, H. Takakura, and A. P. Tsai, Philos. Mag. Lett. **80**, 495 (2000).
[102] I. R. Fisher, X. P. Xie, I. Tudosa, C. W. Gao, C. Song, P. C. Canfield, A. Kracher, K. Dennis, D. Abanoz, and M. J. Kramer, Philos. Mag. B **82**, 1089 (2002).
[103] J. Dolinšek, P. J. McGuiness, M. Klanjšek, I. Smiljanić, A. Smontara, E. S. Zijlstra, S. K. Bose, I. R. Fisher, M. J. Kramer, and P. C. Canfield, Phys. Rev. B **74**, 134201 (2006).